Progress In Electromagnetics Research B, Vol. 21, 347–383, 2010

FLEXIBLE HOLLOW WAVEGUIDE WITH TWO BENDINGS FOR SMALL VALUES OF STEP ANGLES, AND APPLICATIONS

Z. Menachem †

Department of Electrical Engineering
Sami Shamoon College of Engineering
Beer-Sheva 84100, Israel

Abstract—This paper presents an improved approach for the propagation of electromagnetic (EM) fields in the case of the flexible hollow waveguide that consists of two bendings in the same direction. In this case, the objective is to develop a mode model for infrared (IR) wave propagation along the flexible hollow waveguide, in order to provide a numerical tool for the calculation of the output fields, output power density and output power transmission. The main steps of the method for the two bendings will introduced in the derivation, in detail, for small values of step angles. The derivation for the first section and the second section of the waveguide with the two bendings is based on Maxwell's equations. The separation of variables is obtained by using the orthogonal-relations. The longitudinal components of the fields are developed into the Fourier-Bessel series. The transverse components of the fields are expressed as functions of the longitudinal components in the Laplace plane and are obtained by using the inverse Laplace transform by the residue method. This model can be a useful tool in all the cases of the hollow toroidal waveguides, e.g., in medical and industrial regimes.

1. INTRODUCTION

Various methods of cylindrical hollow metallic or metallic with inner dielectric coating waveguide have been proposed in the literature [1–16]. A review of the hollow waveguide technology [1] and a review of IR transmitting, hollow waveguides, fibers and integrated optics [2] were published. The first theoretical analysis of the problem

Corresponding author: Z. Menachem (zionm@post.tau.ac.il).
† Also with Department of Electrical, Electronics, and Communication Engineering, Holon Institute of Technology, 52 Golomb St. POB 305, Israel.

of hollow cylindrical bent waveguides was published by Marcatili and Schmeltzer [3], where the theory considers the bending as a small disturbance and uses cylindrical coordinates to solve Maxwell equations. They derive the mode equations of the disturbed waveguide using the ratio of the inner radius r to the curvature radius R as a small parameter ($r/R \ll 1$). Their theory predicts that the bending has little influence on the attenuation of a hollow metallic waveguide. However, practical experiments have shown a large increase in the attenuation, even for a rather large R.

Marhic [4] proposed a mode-coupling analysis of the bending losses of circular metallic waveguide in the IR range for large bending radii. In the circular guide it is found that the preferred TE_{01} mode can couple very effectively to the lossier TM_{11} mode when the guide undergoes a circular bend. The mode-coupling analysis [4] developed to study bending losses in microwave guides has been applied to IR metallic waveguides at $\lambda = 10.6\,\mu\text{m}$. For circular waveguides, the microwave approximation has been used for the index of refraction and the straight guide losses, and the results indicate very poor bending properties due to the near degeneracy of the TE_{01} and TM_{11} modes, thereby offering an explanation for the high losses observed in practice.

Miyagi et al. [5] suggested an improved solution, which provided agreement with the experimental results, but only for $r/R \ll 1$. A different approach [4, 6] treats the bending as a perturbation that couples the modes of a straight waveguide. That theory explains qualitatively the large difference between the metallic and metallic-dielectric bent waveguide attenuation. The reason for this difference is that in metallic waveguides the coupling between the TE and TM modes caused by the bending mixes modes with very low attenuation and modes with very high attenuation, whereas in metallic-dielectric waveguides, both the TE and TM modes have low attenuation. The EH and HE modes have similar properties and can be related to modes that have a large TM component.

Hollow waveguides with both metallic and dielectric internal layers were proposed to reduce the transmission losses. Hollow-core waveguides have two possibilities. The inner core materials have refractive indices greater than one (namely, leaky waveguides) or the inner wall material has a refractive index of less than one. A hollow waveguide can be made, in principle, from any flexible or rigid tube (plastic, glass, metal, etc.) if its inner hollow surface (the core) is covered by a metallic layer and a dielectric overlayer. This layer structure enables us to transmit both the TE and TM polarization with low attenuation [4, 6].

A method for the EM analysis of bent waveguides [7] is based on

the expansion of the bend mode in modes of the straight waveguides, including the modes under the cutoff. A different approach to calculate the bending losses in curved dielectric waveguides [8] is based on the well-known conformal transformation of the index profile and on vectorial eigenmode expansion combined with perfectly matched layer boundary conditions to accurately model radiation losses. An improved ray model for simulating the transmission of laser radiation through a metallic or metallic dielectric multibent hollow cylindrical waveguide was proposed in [9, 10]. It was shown theoretically and proved experimentally that the transmission of CO_2 radiation is possible even through bent waveguide.

The propagation of EM waves in a loss-free inhomogeneous hollow conducting waveguide with a circular cross section and uniform plane curvature of the longitudinal axis was considered in [11]. For small curvature the field equations can, however, be solved by means of an analytical approximation method. In this approximation the curvature of the axis of the waveguide was considered as a disturbance of the straight circular cylinder, and the perturbed torus field was expanded in eigenfunctions of the unperturbed problem. Using the Rayleigh-Schrodinger perturbation theory, eigenvalues and eigenfunctions containing first-order correction terms were derived. An extensive survey of the related literature can be found especially in the book on EM waves and curved structures [12]. The radiation from curved open structures is mainly considered by using a perturbation approach, that is by treating the curvature as a small perturbation of the straight configuration. The perturbative approach is not entirely suitable for the analysis of relatively sharp bends, such as those required in integrated optics and especially short millimeter waves.

The models based on the perturbation theory consider the bending as a perturbation ($r/R \ll 1$), and solve problems only for a large radius of curvature.

Several methods of propagation along the toroidal and helical waveguides were developed in [13–16], where the derivation is based on Maxwell's equations. The method in [13] has been derived for the analysis of EM wave propagation in dielectric waveguides with arbitrary profiles, with rectangular metal tubes, and along a curved dielectric waveguide. An improved approach has been derived for the propagation of EM field along a toroidal dielectric waveguide with a circular cross-section [14]. The method in [15] has been derived for the propagation of EM field along a helical dielectric waveguide with a circular cross section. The method in [16] has been derived for the propagation of EM field along a helical dielectric waveguide with a rectangular cross section. It is very interesting to compare between

the mode model methods for wave propagation in the waveguide with a rectangular cross section, as proposed in Refs. [13, 16] as regard to the mode model methods for wave propagation in the waveguide with a circular cross section, as proposed in Refs. [14, 15]. The calculations in all the two above methods are based on using Laplace and Fourier transforms, and the output fields are computed by the inverse Laplace and Fourier transforms. Laplace transform on the differential wave equations is needed to obtain the wave equations (and thus also the output fields) that are expressed directly as functions of the transmitted fields at the entrance of the waveguide at $\zeta = 0^+$. Thus, the Laplace transform is necessary to obtain the comfortable and simple *input-output* connections of the fields. The objective in all these methods was to develop a mode model in order to provide a numerical tool for the calculation of the output fields for a curved waveguide. The technique of the methods is quite different. The technique for a rectangular cross section is based on Fourier coefficients of the transverse dielectric profile and those of the input wave profile. On the other hand, the technique for a circular cross section is based on the development of the longitudinal components of the fields into Fourier-Bessel series. The transverse components of the fields are expressed as functions of the longitudinal components in the Laplace plane and are obtained by using the inverse Laplace transform.

The main objective of this paper is to generalize the method [14] to provide a numerical tool for the calculation of the output transverse fields and power density in the case of the flexible hollow waveguide that consists of two bendings. Our method employs toroidal coordinates (and not cylindrical coordinates, such as in the methods that considered the bending as a perturbation ($r/R \ll 1$)). The objective is to presents an improved approach for the propagation of EM fields in the case of the flexible hollow waveguide that consists of two bendings in the same direction. The main steps of the method for the two bendings will introduced in the derivation, in detail, for small values of step angles. The derivation for the first section and the second section of the waveguide with the two bendings is based on Maxwell's equations. The separation of variables is obtained by using the orthogonal-relations. The longitudinal components of the fields are developed into the Fourier-Bessel series. The transverse components of the fields are expressed as functions of the longitudinal components in the Laplace plane and are obtained by using the inverse Laplace transform by the residue method. The results of this model are applied to the study of flexible hollow waveguides with two bendings, that are suitable for transmitting IR radiation, especially CO_2 laser radiation. In this paper, we supposed that the modes excited at the input of the

waveguide by the conventional CO_2 laser IR radiation ($\lambda = 10.6\,\mu m$) are closer to the TEM polarization of the laser radiation. The TEM_{00} mode is the fundamental and the most important mode. This means that a cross-section of the beam has a Gaussian intensity distribution.

2. FORMULATION OF THE PROBLEM

The method presented in [14] is generalized to provide a numerical tool for the calculation of the output transverse fields and power density in the case of the flexible hollow waveguide that consists of two bendings. Let us assume in the derivation that the flexible hollow waveguide consists of two bendings as shown in Fig. 1, in order to simplify the mathematical expressions. The main steps for calculations of the output fields and output power density in the case of the flexible hollow waveguide with two bendings in the same direction (Fig. 1), are introduced in the derivation, in detail.

The coordinates of an arbitrary point on the toroidal system (r, θ, ζ) with a given bending (R) are shown in Fig. 2, where $X = R\cos\phi$ and $Y = R\sin\phi$.

Further we assume that the first bending (Fig. 1) is R_1, the length $\zeta_1 = R_1\phi_1$, and the metric coefficient is $h_{\zeta_1} = 1+(r/R_1)\sin\theta$. Likewise, the radius of curvature of the second bending (Fig. 1) is R_2, the length $\zeta_2 = R_2\phi_2$, and the metric coefficient is $h_{\zeta_2} = 1 + (r/R_2)\sin\theta$. The total length in this case is given by $\zeta = \zeta_1 + \zeta_2$. The cases for a straight waveguide are obtained by letting $R_1 \to \infty$ and $R_2 \to \infty$.

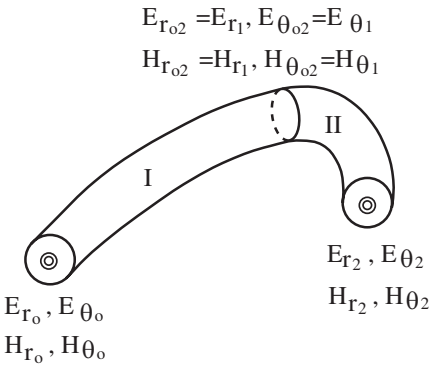

Figure 1. A general scheme in the case that the two bendings are in the same direction.

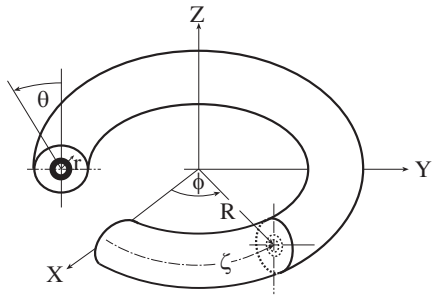

Figure 2. A general scheme of the toroidal system (r, θ, ζ) and the curved waveguide.

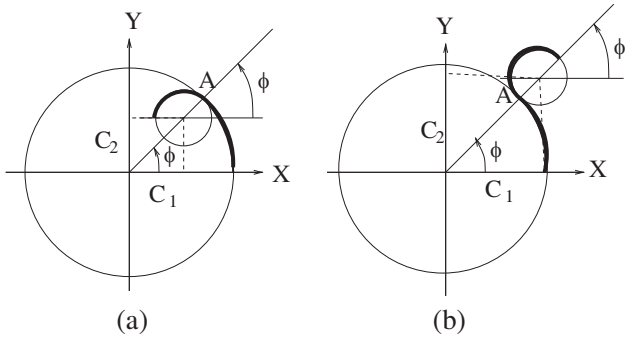

Figure 3. A general scheme of the flexible hollow waveguide with two bendings: (a) In the same direction; (b) in the opposite directions.

A general scheme of the flexible hollow waveguide with two bendings in the same direction is shown in Fig. 3(a). The flexible hollow waveguide with two bendings in the opposite directions is shown in Fig. 3(b).

For the first bending $X = R_1 \cos\phi$, $Y = R_1 \sin\phi$, $dX = -R_1 \sin\phi d\phi$ and $dY = R_1 \cos\phi d\phi$. Thus, the second derivative for the first bending at the point A (Figs. 3(a) and 3(b)) is given by

$$Y''_{(A,R_1)} = \left[\frac{d^2Y}{dX^2}\right]_A = \left[\frac{d}{d\phi}\left(\frac{dY}{dX}\right)\frac{d\phi}{dX}\right]_A = \left[\frac{d}{d\phi}\left(-\cot\phi\right)\left(-\frac{1}{R_1\sin\phi}\right)\right]_A$$
$$= -\frac{1}{R_1 \sin^3\phi_A}.$$

For the second bending at the point A (Figs. 3(a) and 3(b)) the values of X, Y, dX and dY are $X = R_2\cos\phi + c_1$, $Y = R_2\sin\phi + c_2$, $dX = -R_2\sin\phi d\phi$ and $dY = R_2\cos\phi d\phi$, where c_1 and c_2 are denoted in Figs. 3(a) and 3(b). Thus, the second derivative where the two bendings are in the same direction is $Y''_{(A,R_2)} = -1/(R_2\sin^3\phi_A)$. The second derivative at point A, where the two bendings are in the opposite directions is given by $Y''_{(A,R_2)} = +1/(R_2\sin^3(\phi_A + \pi))$.

The second derivative for the first bending at the point A is $Y''_{A,R_1} = -1/R_1$, where $\phi_A = \pi/2$. The second derivative for the second bending at the point A is $y''_{A,R_2} = -1/R_2$, where the two bendings are in the same direction. The difference between the second derivatives at $\phi_A = \pi/2$, in the case of the opposite bendings, is $1/R_1 + 1/R_2$ and in the case of the bendings in the same direction, is $1/R_2 - 1/R_1$. Note that for the same bending ($R_1 = R_2 = R$), the jump of the second derivative at the interface between the two bendings in the

case of the opposite bendings is $2/R$, and in the other case there is no jump. Hence, we introduce the main steps of our method for two different bendings ($R_1 \neq R_2$) for the example as shown in Fig. 1. For the small difference between the bendings ($R_1 \simeq R_2$), the losses in the interface between the two bendings are small. By increasing the difference between the bendings ($R_1 \neq R_2$) the jump of the second derivative at the interface between the two bendings is increased, and therefore the losses are increased.

Let us assume in the derivation that the flexible hollow waveguide consists of two bendings as shown in Fig. 1, in order to simplify the mathematical expressions. The main steps for calculations of the output fields and output power density in the case of the flexible hollow waveguide with two bendings in the same direction (Fig. 1), are introduced in the derivation, in detail.

We start by finding the metric coefficients from the toroidal transformation of the coordinates. The latter will be used in the wave equations as will be outlined in the next section.

The toroidal transformation of the coordinates is achieved by two

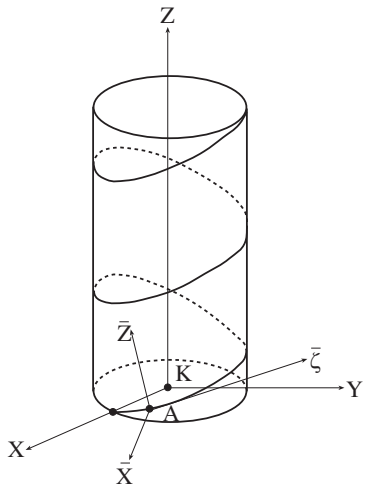

Figure 4. Rotations and translation of the orthogonal system $(\bar{X}, \bar{\zeta}, \bar{Z})$ from point A to the orthogonal system (X, Y, Z) at point K.

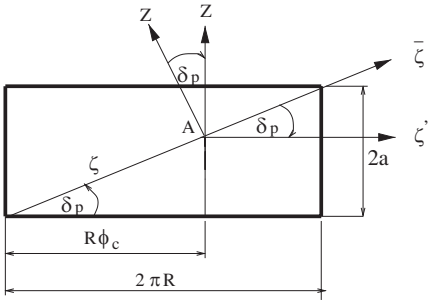

Figure 5. Deployment of the helix.

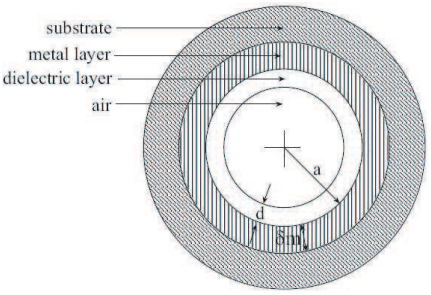

Figure 6. A cross-section of the waveguide (r, θ).

rotations and one translation, and is given in the form:

$$\begin{pmatrix} X \\ Y \\ Z \end{pmatrix} = \begin{pmatrix} \cos(\phi_c) & -\sin(\phi_c) & 0 \\ \sin(\phi_c) & \cos(\phi_c) & 0 \\ 0 & 0 & 1 \end{pmatrix} \begin{pmatrix} 1 & 0 & 0 \\ 0 & \cos(\delta_p) & -\sin(\delta_p) \\ 0 & \sin(\delta_p) & \cos(\delta_p) \end{pmatrix} \begin{pmatrix} r\sin\theta \\ 0 \\ r\cos\theta \end{pmatrix} + \begin{pmatrix} R\cos(\phi_c) \\ R\sin(\phi_c) \\ \zeta\sin(\delta_p) \end{pmatrix}, \quad (1)$$

where ζ is the coordinate along the helix axis, R is the radius of the cylinder, δ_p is the step's angle of the helix (see Figs. 4–5), and $\phi_c = (\zeta\cos(\delta_p))/R$. Likewise, $0 \leq r \leq a + \delta_m$, where $2a$ is the internal diameter of the cross-section of the helical waveguide, δ_m is the thickness of the metallic layer, and d is the thickness of the dielectric layer (see Fig. 6).

Figure 4 shows the rotations and translation of the orthogonal system $(\overline{X}, \overline{\zeta}, \overline{Z})$ from point A to the orthogonal system (X, Y, Z) at point K. In the first rotation, the $\overline{\zeta}$ and $\overline{Z}$ axes rotate around the $\overline{X}$ axis of the orthogonal system $(\overline{X}, \overline{\zeta}, \overline{Z})$ at the point A until the $\overline{Z}$ axis becomes parallel to the Z axis $(\overline{Z} \parallel Z)$, and the $\overline{\zeta}$ axis becomes parallel to the X, Y plane $(\overline{\zeta} \parallel (X, Y))$ of the orthogonal system (X, Y, Z) at the point K. In the second rotation, the $\overline{X}$ and $\overline{\zeta}$ axes rotate around the $\overline{Z}$ axis $(\overline{Z} \parallel Z)$ of the orthogonal system $(\overline{X}, \overline{\zeta}, \overline{Z})$ until $\overline{X} \parallel X$ and $\overline{\zeta} \parallel Y$. After the two above rotations, we have one translation from the orthogonal system $(\overline{X}, \overline{\zeta}, \overline{Z})$ at point A to the orthogonal system (X, Y, Z) at the point K.

Figure 5 shows the deployment of the helix depicted in Fig. 4. The condition for the step's angle δ_p is given according to

$$\tan(\delta_p) \geq \frac{2(a + \delta_m)}{2\pi R}, \quad (2)$$

where the internal diameter is denoted as $2a$, the thickness of the metallic layer is denoted as δ_m, and the radius of the cylinder is denoted as R.

According to Equation (1), the helical transformation of the coordinates becomes

$$X = (R + r\sin\theta)\cos(\phi_c) + r\sin(\delta_p)\cos\theta\sin(\phi_c), \tag{3a}$$

$$Y = (R + r\sin\theta)\sin(\phi_c) - r\sin(\delta_p)\cos\theta\cos(\phi_c), \tag{3b}$$

$$Z = r\cos\theta\cos(\delta_p) + \zeta\sin(\delta_p). \tag{3c}$$

where $\phi_c = (\zeta/R)\cos(\delta_p)$, R is the radius of the cylinder, and (r, θ) are the parameters of the cross-section. Note that $\zeta\sin(\delta_p) = R\phi_c\tan(\delta_p)$.

The metric coefficients in the case of the helical waveguide according to Equations (3a)–(3c) are:

$$h_r = 1, \tag{4a}$$

$$h_\theta = r, \tag{4b}$$

$$h_\zeta = \sqrt{\left(1 + \frac{r}{R}\sin\theta\right)^2\cos^2(\delta_p) + \sin^2(\delta_p)\left(1 + \frac{r^2}{R^2}\cos^2\theta\cos^2(\delta_p)\right)}$$

$$= \sqrt{1 + \frac{2r}{R}\sin\theta\cos^2(\delta_p) + \frac{r^2}{R^2}\sin^2\theta\cos^2(\delta_p) + \frac{r^2}{R^2}\cos^2\theta\cos^2(\delta_p)\sin^2(\delta_p)}$$

$$\simeq 1 + \frac{r}{R}\sin\theta\cos^2(\delta_p). \tag{4c}$$

Furthermore, the third and the fourth terms in the root of the metric coefficient h_ζ are negligible in comparison to the first and the second terms when $(r/R)^2 \ll 1$. Nonetheless, the metric coefficient h_ζ still depends on δ_p, the step's angle of the helix (Fig. 5). Note that the metric coefficient h_ζ is a function of r and θ, which causes a difficulty in the separation of variables. Thus, the analytical methods are not suitable for the helical or the curved waveguide. In this method, the separation of variables is performed by employing the orthogonal-relations. The cross-section of the helical waveguide in the region $0 \le r \le a + \delta_m$ is shown in Fig. 6, where δ_m is the thickness of the metallic layer, and d is the thickness of the dielectric layer.

Further we assume that the derivation based for small values of the step's angle. For small values of the step's angle δ_p ($\sin(\delta_p) \simeq \tan(\delta_p) \simeq \delta_p, \cos(\delta_p) \simeq 1$) and according to condition (2), $\delta_p \ge 2(a + \delta_m)/(2\pi R)$. For small values of the step's angle, the helical waveguide becomes a toroidal waveguide, where the radius of the curvature of the helix can then be approximately by the radius of the cylinder (R). In this case, the toroidal system (r, θ, ζ) in conjunction with the curved waveguide is shown in Fig. 2, and the transformation of the coordinates ((3a)–(3c)) is given as a special case of the toroidal transformation of the

coordinates, as follows

$$X = (R + r\sin\theta)\cos\left(\frac{\zeta}{R}\right), \tag{5a}$$

$$Y = (R + r\sin\theta)\sin\left(\frac{\zeta}{R}\right), \tag{5b}$$

$$Z = r\cos\theta, \tag{5c}$$

and the metric coefficients are given by

$$h_r = 1, \tag{6a}$$

$$h_\theta = r, \tag{6b}$$

$$h_\zeta = 1 + \frac{r}{R}\sin\theta. \tag{6c}$$

By using the Serret-Frenet relations for a spatial curve, we can find the curvature (κ) and the torsion (τ) for each spatial curve that is characterized by $\theta = \text{const}$ and $r = \text{const}$ for each pair (r, θ) in the range. This is achieved by using the helical transformation introduced in Equations (3a), (3b), and (3c). The curvature and the torsion (see Appendix A) are constants for constant values of the radius of the cylinder (R), the step's angle (δ_p) and the parameters (r, θ) of the cross-section. The curvature and the torsion are given by

$$\kappa = \frac{1 + C_t}{R\,(1 + \tan^2(\delta_p) + C_t)}, \tag{7a}$$

$$\tau = \frac{\tan(\delta_p)}{R\,(1 + \tan^2(\delta_p) + C_t)}, \tag{7b}$$

where

$$C_t = \frac{r^2}{R^2}\sin^2\theta + 2\frac{r}{R}\sin\theta + \frac{r^2}{R^2}\sin^2(\delta_p)\cos^2\theta.$$

The radius of curvature and the radius of torsion are given by $\rho = 1/\,\kappa$, and $\sigma = 1/\,\tau$, respectively. For small values of the step's angle ($\delta_p \ll 1$), the helical waveguide becomes a toroidal waveguide (Fig. 2), where the radius of the curvature of the helix can then be approximately by the radius of the cylinder ($\rho \simeq R$).

The generalization of the method from a toroidal dielectric waveguide [14] with one bending to a toroidal dielectric waveguide with two bendings is presented in the following derivation. The derivation is based on Maxwell's equations for the computation of the EM field and the radiation power density at each point during propagation along a helical waveguide, with a radial dielectric profile. The longitudinal components of the fields are developed into the Fourier-Bessel series.

The transverse components of the fields are expressed as a function of the longitudinal components in the Laplace transform domain. Finally, the transverse components of the fields are obtained by using the inverse Laplace transform by the residue method, for small values of the step's angles. The main steps of the method for the two bendings in the same direction (Fig. 1) will introduced in the following derivation, in detail.

3. SOLUTION OF THE WAVE EQUATIONS

The wave equations for the electric and magnetic field components in the inhomogeneous dielectric medium $\epsilon(r)$ are derived in this section for a lossy dielectric media in metallic boundaries of the waveguide. The cross-section of the toroidal waveguide is shown in Fig. 6 for the application of the hollow waveguide, in the region $0 \leq r \leq a + \delta_m$, where δ_m is the thickness of the metallic layer, and d is the thickness of the dielectric layer.

The derivation is given for the lossless case to simplify the mathematical expressions. In a linear lossy medium, the solution is obtained by replacing the permittivity ϵ by $\epsilon_c = \epsilon - j(\sigma/\omega)$ in the solutions for the lossless case, where ϵ_c is the complex dielectric constant, and σ is the conductivity of the medium. The boundary conditions for a lossy medium are given after the derivation. For most materials, the permeability μ is equal to that of free space ($\mu = \mu_0$). The wave equations for the electric and magnetic field components in the inhomogeneous dielectric medium $\epsilon(r)$ are given by

$$\nabla^2\mathbf{E} + \omega^2\mu\epsilon\mathbf{E} + \nabla\left(\mathbf{E}\cdot\frac{\nabla\epsilon}{\epsilon}\right) = 0, \tag{8a}$$

and

$$\nabla^2\mathbf{H} + \omega^2\mu\epsilon\mathbf{H} + \frac{\nabla\epsilon}{\epsilon}\times(\nabla\times\mathbf{H}) = 0, \tag{8b}$$

respectively. The transverse dielectric profile ($\epsilon(r)$) is defined as $\epsilon_0(1 + g(r))$, where ϵ_0 represents the vacuum dielectric constant, and $g(r)$ is its profile function in the waveguide. The normalized transverse derivative of the dielectric profile (g_r) is defined as $(1/\epsilon(r))(\partial\epsilon(r)/\partial r)$.

From the transformation of Equations (3a)–(3c) we can derive the Laplacian of the vector $\mathbf{E}$ (i.e., $\nabla^2\mathbf{E}$), and obtain the wave equations for the electric and magnetic fields in the inhomogeneous dielectric medium. It is necessary to find the values of $\nabla\cdot\mathbf{E}$, $\nabla(\nabla\cdot\mathbf{E})$, $\nabla\times\mathbf{E}$, and $\nabla\times(\nabla\times\mathbf{E})$ in order to obtain the value of $\nabla^2\mathbf{E}$, where $\nabla^2\mathbf{E} = \nabla(\nabla\cdot\mathbf{E}) - \nabla\times(\nabla\times\mathbf{E})$. All these values are dependent on the metric coefficients (4a), (4b) and (4c).

The ζ component of $\nabla^2\mathbf{E}$ is given by

$$\left(\nabla^2\mathbf{E}\right)_\zeta = \nabla^2 E_\zeta + \frac{2}{Rh_\zeta^2}\left[\sin\theta\frac{\partial}{\partial\zeta}E_r + \cos\theta\frac{\partial}{\partial\zeta}E_\theta\right] - \frac{1}{R^2h_\zeta^2}E_\zeta, \quad (9)$$

where

$$\begin{aligned}\nabla^2 E_\zeta \;=\; & \frac{\partial^2}{\partial r^2}E_\zeta + \frac{1}{r^2}\frac{\partial^2}{\partial\theta^2}E_\zeta + \frac{1}{r}\frac{\partial}{\partial r}E_\zeta \\ & + \frac{1}{h_\zeta}\left[\frac{\sin\theta}{R}\frac{\partial}{\partial r}E_\zeta + \frac{\cos\theta}{rR}\frac{\partial}{\partial\theta}E_\zeta + \frac{1}{h_\zeta}\frac{\partial^2}{\partial\zeta^2}E_\zeta\right]. \quad (10)\end{aligned}$$

The longitudinal components of the wave Equations (8a) and (8b) are obtained by deriving the following terms

$$\left[\nabla\left(\mathbf{E}\cdot\frac{\nabla\epsilon}{\epsilon}\right)\right]_\zeta = \frac{1}{h_\zeta}\frac{\partial}{\partial\zeta}\left[E_r g_r\right], \quad (11)$$

and

$$\left[\frac{\nabla\epsilon}{\epsilon}\times(\nabla\times\mathbf{H})\right]_\zeta = j\omega\epsilon\left[\frac{\nabla\epsilon}{\epsilon}\times\mathbf{E}\right]_\zeta = j\omega\epsilon g_r E_\theta. \quad (12)$$

The longitudinal components of the wave Equations (8a) and (8b) are then written in the form

$$\left(\nabla^2\mathbf{E}\right)_\zeta + k^2 E_\zeta + \frac{1}{h_\zeta}\frac{\partial}{\partial\zeta}\left(E_r g_r\right) = 0, \quad (13)$$

$$\left(\nabla^2\mathbf{H}\right)_\zeta + k^2 H_\zeta + j\omega\epsilon g_r E_\theta = 0, \quad (14)$$

where $(\nabla^2\mathbf{E})_\zeta$, for instance, is given in Equation (9). The *local* wave number parameter is $k = \omega\sqrt{\mu\epsilon(r)} = k_0\sqrt{1+g(r)}$, where the free-space wave number is $k_0 = \omega\sqrt{\mu_0\epsilon_0}$.

The transverse Laplacian operator is defined as

$$\nabla_\perp^2 \equiv \nabla^2 - \frac{1}{h_\zeta^2}\frac{\partial^2}{\partial\zeta^2}. \quad (15)$$

The Laplace transform

$$\tilde{a}(s) = \mathcal{L}\{a(\zeta)\} = \int_{\zeta=0}^{\infty} a(\zeta)e^{-s\zeta}d\zeta \quad (16)$$

is applied on the ζ-dimension, where $a(\zeta)$ represents any ζ-dependent variables, where $\zeta = (R\phi_c)/\cos(\delta_p)$.

The next steps are given in detail in Ref. [14], as a part of our derivation. Let us repeat these main steps, in brief. By substituting Equation (9) into Equation (13) and by using the Laplace transform (16), the longitudinal components of the wave equations (Equations (13)–(14)) are described in the Laplace transform domain, as *coupled* wave equations. The transverse fields for the first section of the flexible hollow waveguide with two bendings at $\zeta = \zeta_1$ are obtained directly from the Maxwell equations, and by using the Laplace transform (16), and are given by

$$\tilde{E}_{r_1}(s) = \frac{1}{s^2 + k^2 h_{\zeta_1}^2} \left\{ -\frac{j\omega\mu_0}{r} \left[\frac{r}{R_1} \cos\theta \tilde{H}_{\zeta_1} + h_{\zeta_1} \frac{\partial}{\partial\theta} \tilde{H}_{\zeta_1} \right] h_{\zeta_1} + s \left[\frac{\sin\theta}{R_1} \tilde{E}_{\zeta_1} + h_{\zeta_1} \frac{\partial}{\partial r} \tilde{E}_{\zeta_1} \right] + sE_{r_0} - j\omega\mu_0 H_{\theta_0} h_{\zeta_1} \right\}. \quad (17a)$$

$$\tilde{E}_{\theta_1}(s) = \frac{1}{s^2 + k^2 h_{\zeta_1}^2} \left\{ \frac{s}{r} \left[\frac{r}{R_1} \cos\theta \tilde{E}_{\zeta_1} + h_{\zeta_1} \frac{\partial}{\partial\theta} \tilde{E}_{\zeta_1} \right] + j\omega\mu_0 h_{\zeta_1} \left[\frac{\sin\theta}{R_1} \tilde{H}_{\zeta_1} + h_{\zeta_1} \frac{\partial}{\partial r} \tilde{H}_{\zeta_1} \right] + sE_{\theta_0} + j\omega\mu_0 H_{r_0} h_{\zeta_1} \right\}, \quad (17b)$$

$$\tilde{H}_{r_1}(s) = \frac{1}{s^2 + k^2 h_{\zeta_1}^2} \left\{ \frac{j\omega\epsilon}{r} \left[\frac{r}{R_1} \cos\theta \tilde{E}_{\zeta_1} + h_{\zeta_1} \frac{\partial}{\partial\theta} \tilde{E}_{\zeta_1} \right] h_{\zeta_1} + s \left[\frac{\sin\theta}{R_1} \tilde{H}_{\zeta_1} + h_{\zeta_1} \frac{\partial}{\partial r} \tilde{H}_{\zeta_1} \right] + sH_{r_0} + j\omega\epsilon E_{\theta_0} h_{\zeta_1} \right\}, \quad (17c)$$

$$\tilde{H}_{\theta_1}(s) = \frac{1}{s^2 + k^2 h_{\zeta_1}^2} \left\{ \frac{s}{r} \left[\frac{r}{R_1} \cos\theta \tilde{H}_{\zeta_1} + h_{\zeta_1} \frac{\partial}{\partial\theta} \tilde{H}_{\zeta_1} \right] - j\omega\epsilon h_{\zeta_1} \left[\frac{\sin\theta}{R_1} \tilde{E}_{\zeta_1} + h_{\zeta_1} \frac{\partial}{\partial r} \tilde{E}_{\zeta_1} \right] + sH_{\theta_0} - j\omega\epsilon E_{r_0} h_{\zeta_1} \right\}, \quad (17d)$$

where ζ_1 is the coordinate along the first section toroidal axis, R_1 is the radius of curvature of the first section of the toroidal axis, where the metric coefficient is $h_{\zeta_1} = 1 + (r/R_1)\sin\theta$.

The transverse fields are substituted into the *coupled* wave equations. The longitudinal components of the fields are developed into Fourier-Bessel series, in order to satisfy the metallic boundary conditions of the circular cross-section. The condition is that we have only ideal boundary conditions for $r = a$. Thus, the electric and magnetic fields will be zero in the metal. Two sets of equations are obtained by substitution the longitudinal components of the fields

into the wave equations. The first set of the equations is multiplied by $\cos(n\theta)J_n(P_{nm}r/a)$, and after that by $\sin(n\theta)J_n(P_{nm}r/a)$, for $n \neq 0$. Similarly, the second set of the equations is multiplied by $\cos(n\theta)J_n(P'_{nm}r/a)$, and after that by $\sin(n\theta)J_n(P'_{nm}r/a)$, for $n \neq 0$. In order to find an algebraic system of four equations with four unknowns, it is necessary to integrate over the area (r, θ), where $r = [0, a]$, and $\theta = [0, 2\pi]$, by using the orthogonal-relations of the trigonometric functions. The propagation constants β_{nm} and β'_{nm} of the TM and TE modes of the hollow waveguide [17] are given, respectively, by $\beta_{nm} = \sqrt{k_o^2 - (P_{nm}/a)^2}$ and $\beta'_{nm} = \sqrt{k_o^2 - (P'_{nm}/a)^2}$, where the transverse Laplacian operator $(\nabla_\perp^2)$ is given by $-(P_{nm}/a)^2$ and $-(P'_{nm}/a)^2$ for the TM and TE modes of the hollow waveguide, respectively.

3.1. The Elements of the Boundary Conditions's Vectors in the Entrance of the First Section of the Toroidal Waveguide

The separation of variables is obtained by using the orthogonal-relations. Thus the algebraic equations $(n \neq 0)$ are given by

$$\alpha_n{}^{(1)}A_n + \beta_n{}^{(1)}D_n = \frac{1}{\pi}\widehat{(BC1)}_n, \tag{18a}$$

$$\alpha_n{}^{(2)}B_n + \beta_n{}^{(2)}C_n = \frac{1}{\pi}\widehat{(BC2)}_n, \tag{18b}$$

$$\beta_n{}^{(3)}B_n + \alpha_n{}^{(3)}C_n = \frac{1}{\pi}\widehat{(BC3)}_n, \tag{18c}$$

$$\beta_n{}^{(4)}A_n + \alpha_n{}^{(4)}D_n = \frac{1}{\pi}\widehat{(BC4)}_n. \tag{18d}$$

Further we assume $n' = n = 1$. The elements $(\alpha_n{}^{(1)}, \beta_n{}^{(1)}$, etc), on the left side of (18a) for $n = 1$ are given for the first section of the toroidal waveguide by:

$$\alpha_1{}^{(1)mm'} = \pi\left(s^2 + \beta_{1m'}^2\right)\left[\left(s^2 + {k_0}^2\right)G_{00}^{(1)mm'} + {k_0}^2 G_{01}^{(1)mm'}\right]$$

$$+\pi {k_0}^2\left\{s^2 G_{01}^{(1)mm'} + G_{05}^{(1)mm'} + \frac{1}{R_1^2}\left(G_{00}^{(1)mm'} + G_{01}^{(1)mm'}\right)\right.$$

$$\left.+\frac{3}{2R_1^2}\beta_{1m'}^2\left(G_{02}^{(1)mm'} + G_{03}^{(1)mm'}\right) + \pi s^2\left[G_{08}^{(1)mm'} + \frac{1}{2R_1^2}G_{00}^{(1)mm'}\right.\right.$$

$$+\frac{1}{4R_1^2}\left(\beta_{1m'}^2 G_{02}^{(1)mm'}+G_{09}^{(1)mm'}\right)+\frac{1}{2R_1^2}\frac{P_{1m'}}{a}\left(G_{10}^{(1)mm'}+\frac{1}{2}G_{11}^{(1)mm'}\right)\Bigg]$$
$$+\pi {k_0}^4\left[\frac{3}{2R_1^2}\left(G_{03}^{(1)mm'}+G_{04}^{(1)mm'}\right)\right], \tag{19a}$$

$${\beta_1}^{(1)mm'}=-j\omega\mu_0\pi s\Bigg\{G_{13}^{(1)mm'}+\left(\frac{5}{4}\right)\frac{1}{R_1^2}G_{14}^{(1)mm'}+\left(\frac{3}{2}\right)\frac{1}{R_1^2}G_{15}^{(1)mm'}$$
$$-\frac{1}{2R_1^2}G_{00}^{(1)mm'}-\frac{1}{R_1^2}\frac{{P'}_{1m'}}{a}G_{16}^{(1)mm'}\Bigg\}, \tag{19b}$$

where the elements of the matrices ($G_{00}^{(1)mm'}$, etc.) are given in Appendix B. Similarly, the rest of the elements on the left side in Equations (18a)–(18d) are obtained. We establish an algebraic system of four equations with four unknowns. All the elements of the matrices in the Laplace transform domain are dependent on the step's angle of the helix (δ_p), the Bessel functions; the dielectric profile $g(r)$; the transverse derivative $g_r(r)$; and $(r,\, \theta)$.

The elements of the boundary conditions's vectors on the right side in Equations (18a)–(18d) are changed at the entrance of every section of the flexible hollow waveguide with two bendings. These elements are given in conjunction with the excitation of every section, as follows:

$$\widehat{(BC1)}_1 = \int_0^{2\pi}\int_0^a (BC1)\cos(\theta)J_1(P_{1m}r/a)rdrd\theta, \tag{20a}$$

$$\widehat{(BC2)}_1 = \int_0^{2\pi}\int_0^a (BC2)\sin(\theta)J_1(P_{1m}r/a)rdrd\theta, \tag{20b}$$

$$\widehat{(BC3)}_1 = \int_0^{2\pi}\int_0^a (BC3)\cos(\theta)J_1({P'}_{1m}r/a)rdrd\theta, \tag{20c}$$

$$\widehat{(BC4)}_1 = \int_0^{2\pi}\int_0^a (BC4)\sin(\theta)J_1({P'}_{1m}r/a)rdrd\theta. \tag{20d}$$

The elements of the boundary conditions's vectors (20a)–(20d) in the case of the TEM_{00} mode in excitation for the first section of the toroidal waveguide with two bendings (Fig. 1) are obtained, where:

$$BC1 = BC2 = j\omega\mu_0 H_{\theta_0}^+ s g_r h_{\zeta_1}^2+\frac{2}{R_1}h_{\zeta_1}\sin\theta\left(j\omega\mu_0 H_{\theta_0}^+ s+k^2 E_{r_0}^+ h_{\zeta_1}\right)$$
$$+\frac{2}{R_1}h_{\zeta_1}\cos\theta\left(-j\omega\mu_0 H_{r_0}^+ s+k^2 E_{\theta_0}^+ h_{\zeta_1}\right)+k^2 h_{\zeta_1}^3 E_{r_0}^+ g_r, \tag{21a}$$

$$BC3 = BC4 = -j\omega\epsilon E^+_{\theta_0} s g_r h^2_{\zeta_1} + \frac{2}{R_1} h_{\zeta_1} \sin\theta \left(k^2 h_{\zeta_1} H^+_{r_0} - j\omega\epsilon s E^+_{\theta_0} \right)$$
$$+ \frac{2}{R_1} h_{\zeta_1} \cos\theta \left(k^2 h_{\zeta_1} H^+_{\theta_0} + j\omega\epsilon s E^+_{r_0} \right) + k^2 h^3_{\zeta_1} H^+_{r_0} g_r. \qquad (21b)$$

The elements of the boundary conditions (e.g., $\widehat{(BC2)}_1$) at $\zeta = 0^+$ on the right side in (18b) are given, where

$$(BC2)_1 = \left[\left(s^2 + k^2 h^2_{\zeta_1} \right) \left(s E_{\zeta_0} + E'_{\zeta_0} \right) \right] + j\omega\mu_0 H_{\theta_0} s g_r h^2_{\zeta_1}$$
$$+ \frac{2}{R_1} h_{\zeta_1} \sin\theta \left(j\omega\mu_0 H_{\theta_0} s + k^2 E_{r_0} h_{\zeta_1} \right)$$
$$+ \frac{2}{R_1} h_{\zeta_1} \cos\theta \left(- j\omega\mu_0 H_{r_0} s + k^2 E_{\theta_0} h_{\zeta_1} \right) + k^2 h^3_{\zeta_1} E_{r_0} g_r.$$

The boundary conditions at $\zeta_1 = 0^+$ for TEM_{00} mode in excitation become to:

$$\widehat{(BC2)}_1 = 2\pi \left\{ \int_0^a Q(r)(k(r) + js) J_{1m}(P_{1m} r/a) r dr \right\} \delta_{1n}$$
$$+ \frac{4js\pi}{R_1^2} \left\{ \int_0^a Q(r) k(r) J_{1m}(P_{1m} r/a) r^2 dr \right\} \delta_{1n}$$
$$+ \frac{9\pi}{2R_1^2} \left\{ \int_0^a Q(r) k^2(r) J_{1m}(P_{1m} r/a) r^3 dr \right\} \delta_{1n}$$
$$+ \frac{3js\pi}{2R_1^2} \left\{ \int_0^a Q(r) k(r) J_{1m}(P_{1m} r/a) r^3 dr \right\} \delta_{1n}$$
$$+ \frac{8\pi}{R_1^2} \left\{ \int_0^a Q(r) k^2(r) J_{1m}(P_{1m} r/a) r^2 dr \right\} \delta_{1n} \qquad (22)$$

where :

$$Q(r) = \frac{E_0}{n_c(r) + 1} g_r \exp\left(-(r/w_o)^2\right).$$

Similarly, the remaining elements of the boundary conditions at $\zeta = 0^+$ are obtained. The matrix system of Equations (18a)–(18d) is solved to obtain the coefficients (A_1, B_1, etc).

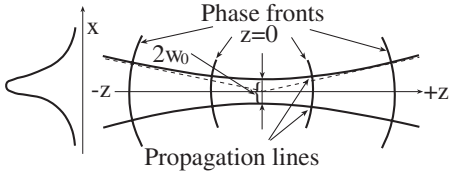

Figure 7. Propagating Gaussian beam.

According to the Gaussian beams [18] the parameter w_0 is the minimum spot-size at the plane $z = 0$ (see Fig. 7), and the electric field at the plane $z = 0$ is given by $E = E_0 \exp[-(r/w_o)^2]$. The modes excited at $\zeta = 0$ in the waveguide by the conventional CO_2 laser IR radiation ($\lambda = 10.6\,\mu$m) are closer to the TEM polarization of the laser radiation. The TEM_{00} mode is the fundamental and most important mode. This means that a cross-section of the beam has a Gaussian intensity distribution. The relation between the electric and magnetic fields [18] is given by $E/H = \sqrt{\mu_0/\epsilon_0} \equiv \eta_0$, where η_0 is the intrinsic wave impedance. Suppose that the electric field is parallel to the y-axis. Thus the components of E_y and H_x are written by the fields $E_y = E_0 \exp[-(r/w_o)^2]$ and $H_x = -(E_0/\eta_0) \exp[-(r/w_o)^2]$.

After a Gaussian beam passes through a lens and before it enters to the waveguide, the waist cross-sectional diameter ($2w_0$) can then be approximately calculated for a parallel incident beam by means of $w_0 = \lambda/(\pi\theta) \simeq (f\lambda)/(\pi w)$. This approximation is justified if the parameter w_0 is much larger than the wavelength λ. The parameter of the waist cross-sectional diameter ($2w_0$) is taken into account in our method, instead of the focal length of the lens (f). The initial fields at $\zeta = 0^+$ are formulated by using the Fresnel coefficients of the transmitted fields [19] as follows

$$E^+_{r_0}\left(r,\theta,\zeta=0^+\right) = T_E(r)\left(E_0 e^{-(r/w_o)^2}\sin\theta\right), \tag{23a}$$

$$E^+_{\theta_0}\left(r,\theta,\zeta=0^+\right) = T_E(r)\left(E_0 e^{-(r/w_o)^2}\cos\theta\right), \tag{23b}$$

$$H^+_{r_0}\left(r,\theta,\zeta=0^+\right) = -T_H(r)\left((E_0/\eta_0)\, e^{-(r/w_o)^2}\cos\theta\right), \tag{23c}$$

$$H^+_{\theta_0}\left(r,\theta,\zeta=0^+\right) = T_H(r)\left((E_0/\eta_0)\, e^{-(r/w_o)^2}\sin\theta\right), \tag{23d}$$

where $E^+_{\zeta_0}(r) = H^+_{\zeta_0} = 0$, $T_E(r) = 2/[n(r)+1]$, $T_H(r) = 2n(r)/[n(r)+1]$, and $n(r) = (\epsilon_r(r))^{1/2}$. The index of refraction is denoted by $n(r)$.

3.2. The Transverse Components of the Fields of the First Section of the Toroidal Waveguide, at $\zeta = \zeta_1$

The transverse components of the fields are finally expressed in a form of *transfer matrix functions* for the first bending of the flexible hollow waveguide as follows:

$$E_{r_1}(r,\theta,\zeta_1) = E_{r0}^{+}(r)e^{-jkh_{\zeta_1}\zeta} - \frac{j\omega\mu_0}{R_1}h_{\zeta_1}\cos^2\theta\sum_{m'}C_{S1}^{m'}(\zeta_1)J_1(\psi)$$
$$-\frac{j\omega\mu_0}{R_1}h_{\zeta_1}\sin\theta\cos\theta\sum_{m'}D_{S1}^{m'}(\zeta_1)J_1(\psi)+\frac{j\omega\mu_0}{r}h_{\zeta_1}^2\sin\theta\sum_{m'}C_{S1}^{m'}(\zeta_1)J_1(\psi)$$
$$-\frac{j\omega\mu_0}{r}h_{\zeta_1}^2\cos\theta\sum_{m'}D_{S1}^{m'}(\zeta_1)J_1(\psi)+\frac{1}{R_1}\sin\theta\cos\theta\sum_{m'}A_{S2}^{m'}(\zeta_1)J_1(\xi)$$
$$+\frac{1}{R_1}\sin^2\theta\sum_{m'}B_{S2}^{m'}(\zeta_1)J_1(\xi)+h_{\zeta_1}\cos\theta\sum_{m'}A_{S2}^{m'}(\zeta_1)\frac{dJ_1}{dr}(\xi)$$
$$+h_{\zeta}\sin\theta\sum_{m'}B_{S2}^{m'}(\zeta_1)\frac{dJ_1}{dr}(\xi), \tag{24}$$

where $h_{\zeta_1} = 1 + (r/R_1)\sin\theta$, R is the radius of the cylinder, δ_p is the the step's angle, $\psi = [P'_{1m'}(r/a)]$ and $\xi = [P_{1m'}(r/a)]$. The coefficients are given in the above equation, for instance

$$A_{S1}^{m'}(\zeta_1) = \mathcal{L}^{-1}\left\{\frac{A_{1m'}(s)}{s^2 + k^2(r)h_{\zeta_1}^2}\right\}, \tag{25a}$$

$$A_{S2}^{m'}(\zeta_1) = \mathcal{L}^{-1}\left\{\frac{sA_{1m'}(s)}{s^2 + k^2(r)h_{\zeta_1}^2}\right\}, \tag{25b}$$

where

$$m' = 1, \ldots N, \qquad 3 \le N \le 50. \tag{25c}$$

Similarly, the other transverse components of the output fields are obtained. The first fifty roots (zeros) of the equations $J_1(x) = 0$ and $dJ_1(x)/dx = 0$ may be found in tables [20, 21].

3.3. The Elements of the Boundary Conditions's Vectors in the Entrance of the Second Section at $\zeta = \zeta_1$

The elements of the boundary conditions's vectors (20a)–(20d) in the case of the TEM_{00} mode in excitation for the second section of the toroidal waveguide with two bendings are obtained from the algebraic

system of Equations (18a)–(18d) for $n = 1$, as follows:

$$\begin{aligned} BC1 \;=\; & BC2 = j\omega\mu_0 H_\theta(\zeta=\zeta_1) s g_r h_{\zeta_2}^2 \\ & + \frac{2}{R_2}\sin\theta h_{\zeta_2}\left(j\omega\mu_0 H_\theta(\zeta=\zeta_1)s + k^2 E_r(\zeta=\zeta_1) h_{\zeta_2}\right) \\ & + \frac{2}{R_2}\cos\theta h_{\zeta_2}\left(- j\omega\mu_0 H_r(\zeta=\zeta_1)s + k^2 E_\theta(\zeta=\zeta_1) h_{\zeta_2}\right) \\ & + k^2 h_{\zeta_2}^3 E_r(\zeta=\zeta_1) g_r, \end{aligned} \tag{26a}$$

$$\begin{aligned} BC3 \;=\; & BC4 = -j\omega\epsilon E_\theta(\zeta=\zeta_1) s g_r h_{\zeta_2}^2 \\ & + \frac{2}{R_2}\sin\theta h_{\zeta_2}\left(k^2 h_{\zeta_2} H_r(\zeta=\zeta_1) - j\omega\epsilon s E_\theta(\zeta=\zeta_1)\right) \\ & + \frac{2}{R_2}\cos\theta h_{\zeta_2}\left(k^2 h_{\zeta_2} H_\theta(\zeta=\zeta_1) + j\omega\epsilon s E_r(\zeta=\zeta_1)\right) \\ & + k^2 h_{\zeta_2}^3 H_r(\zeta=\zeta_1) g_r. \end{aligned} \tag{26b}$$

Equations (26a)–(26b) are different from Equations (21a)–(21b) by the initial fields. The initial field, for instance, at the entrance of the first section at $\zeta = 0^+$ is denoted as $E_{r_0}^+$ according to (23a), but the initial field of the second section in the entrance, at $\zeta = \zeta_1$, is denoted as $E_r(\zeta = \zeta_1)$, according to (24). Similarly, the remaining initial fields are obtained.

The elements of the boundary conditions's vectors (Equations (26a)–(26b)) for the second section of the flexible hollow waveguide with two bendings become

$$\begin{aligned} BC1 = BC2 = & \left[k^2 h_{\zeta_2}^3 g_r + \frac{2}{R_2}\sin\theta h_{\zeta_2}^2 k^2 \right] \left[-\frac{j\omega\mu_0}{R_1} h_{\zeta_1}\cos^2\theta \right. \\ & \sum_{m'} C_{S1}^{m'}(\zeta_1) J_1(\psi) - \frac{j\omega\mu_0}{R_1} h_{\zeta_1}\sin\theta\cos\theta \sum_{m'} D_{S1}^{m'}(\zeta_1) J_1(\psi) \\ & - \frac{j\omega\mu_0}{r} h_{\zeta_1}^2 \cos\theta \sum_{m'} D_{S1}^{m'}(\zeta_1) J_1(\psi) \\ & \left. + \frac{1}{R_1}\sin\theta\cos\theta \sum_{m'} A_{S2}^{m'}(\zeta_1) J_1(\xi) + h_{\zeta_1}\cos\theta \sum_{m'} A_{S2}^{m'}(\zeta_1)\frac{dJ_1}{dr}(\xi) \right] \end{aligned}$$

$$+\left[\frac{2}{R_2}\cos\theta h_{\zeta_2}^2 k^2\right]\left[\frac{j\omega\mu_0}{R_1}h_{\zeta_1}\sin\theta\cos\theta\sum_{m'}C_{S1}^{m'}(\zeta_1)J_1(\psi)\right.$$
$$+\frac{j\omega\mu_0}{R_1}h_{\zeta_1}\sin^2\theta\sum_{m'}D_{S1}^{m'}(\zeta_1)J_1(\psi)+j\omega\mu_0 h_{\zeta_1}^2\sin\theta\sum_{m'}D_{S1}^{m'}(\zeta_1)\frac{dJ_1}{dr}(\psi)$$
$$\left.+\frac{\cos^2\theta}{R_1}\sum_{m'}A_{S2}^{m'}(\zeta_1)J_1(\xi)-\frac{1}{r}h_{\zeta_1}\sin\theta\sum_{m'}A_{S2}^{m'}(\zeta_1)J_1(\xi)\right]$$
$$-\left[\frac{2}{R_2}\cos\theta h_{\zeta_2}j\omega\mu_0 s\right]\left[\frac{j\omega\epsilon}{R_1}h_{\zeta_1}\cos^2\theta\sum_{m'}A_{S1}{}^{m'}(\zeta_1)J_1(\xi)\right.$$
$$-\frac{j\omega\epsilon}{r}h_{\zeta_1}^2\sin\theta\sum_{m'}A_{S1}{}^{m'}(\zeta_1)J_1(\xi)+\frac{1}{R_1}\sin^2\theta\sum_{m'}D_{S2}^{m'}(\zeta_1)J_1(\psi)$$
$$\left.+h_{\zeta_1}\sin\theta\sum_{m'}D_{S2}^{m'}(\zeta_1)\frac{dJ_1}{dr}(\psi)\right]+\left[j\omega\mu_0 s g_r h_{\zeta_2}^2+\frac{2}{R_2}\sin\theta h_{\zeta_2}j\omega\mu_0 s\right]$$
$$\left[-\frac{j\omega\epsilon}{R_1}h_{\zeta_1}\sin\theta\cos\theta\sum_{m'}A_{S1}{}^{m'}(\zeta_1)J_1(\xi)-j\omega\epsilon h_{\zeta_1}^2\cos\theta\sum_{m'}A_{S1}^{m'}(\zeta_1)\frac{dJ_1}{dr}(\xi)\right.$$
$$\left.+\frac{\sin\theta\cos\theta}{R_1}\sum_{m'}D_{S2}^{m'}(\zeta_1)J_1(\psi)+\frac{1}{r}h_{\zeta_1}\cos\theta\sum_{m'}D_{S2}^{m'}(\zeta_1)J_1(\psi)\right],\quad(27a)$$

$$BC3=BC4=\left[\frac{2}{R_2}\cos\theta h_{\zeta_2}j\omega\epsilon s\right]\left[-\frac{j\omega\mu_0}{R_1}h_{\zeta_1}\sin\theta\cos\theta\sum_{m'}D_{S1}^{m'}(\zeta_1)J_1(\psi)\right.$$
$$-\frac{j\omega\mu_0}{r}h_{\zeta_1}^2\cos\theta\sum_{m'}D_{S1}^{m'}(\zeta_1)J_1(\psi)+\frac{1}{R_1}\sin\theta\cos\theta\sum_{m'}A_{S2}^{m'}(\zeta_1)J_1(\xi)$$
$$\left.+h_{\zeta_1}\cos\theta\sum_{m'}A_{S2}^{m'}(\zeta_1)\frac{dJ_1}{dr}(\xi)\right]-\left[j\omega\epsilon s g_r h_{\zeta_2}^2+\frac{2}{R_2}\sin\theta h_{\zeta_2}j\omega\epsilon s\right]$$
$$\left[\frac{j\omega\mu_0}{R_1}h_{\zeta_1}\sin^2\theta\sum_{m'}D_{S1}^{m'}(\zeta_1)J_1(\psi)+j\omega\mu_0 h_{\zeta_1}^2\sin\theta\sum_{m'}D_{S1}^{m'}(\zeta_1)\frac{dJ_1}{dr}(\xi)\right.$$
$$\left.+\frac{\cos^2\theta}{R_1}\sum_{m'}A_{S2}^{m'}(\zeta_1)J_1(\xi)-\frac{1}{r}h_{\zeta_1}\sin\theta\sum_{m'}A_{S2}^{m'}(\zeta_1)J_1(\xi)\right]$$

$$+\left[k^2h_{\zeta_2}^3g_r+\frac{2}{R_2}\sin\theta h_{\zeta_2}^2k^2\right]\left[\frac{j\omega\epsilon}{R_1}h_{\zeta_1}\cos^2\theta\sum_{m'}A_{S1}{}^{m'}(\zeta_1)J_1(\xi)\right.$$
$$-\frac{j\omega\epsilon}{r}h_{\zeta_1}^2\sin\theta\sum_{m'}A_{S1}{}^{m'}(\zeta_1)J_1(\xi)+\frac{1}{R_1}\sin^2\theta\sum_{m'}D_{S2}^{m'}(\zeta_1)J_1(\psi)$$
$$\left.+h_{\zeta_1}\sin\theta\sum_{m'}D_{S2}^{m'}(\zeta_1)\frac{dJ_1}{dr}(\psi)\right]+\left[\frac{2}{R_2}\cos\theta h_{\zeta_2}^2k^2\right]\left[-\frac{j\omega\epsilon}{R_1}h_{\zeta_1}\sin\theta\cos\theta\right.$$
$$\sum_{m'}A_{S1}{}^{m'}(\zeta_1)J_1(\xi)-j\omega\epsilon h_{\zeta_1}^2\cos\theta\sum_{m'}A_{S1}^{m'}(\zeta_1)\frac{dJ_1}{dr}(\xi)$$
$$\left.+\frac{\sin\theta\cos\theta}{R_1}\sum_{m'}D_{S2}^{m'}(\zeta_1)J_1(\psi)+\frac{1}{r}h_{\zeta_1}\cos\theta\sum_{m'}D_{S2}^{m'}(\zeta_1)J_1(\psi)\right]. \quad (27b)$$

These expressions (27a), (27b) are dependent on the radius of curvature of the first section (R_1) and the second section (R_2) of the flexible hollow waveguide with two bendings ($R_1 \neq R_2$). Actually, the expressions (27a), (27b) of the elements of the boundary conditions's vectors of the second section of the flexible waveguide with two bendings consist of all the information at the output fields of the first section (the Bessel-equations, the dielectric profile $g(r)$, the transverse derivative $g_r(r)$, the parameters of the cross-section (r, θ), and the propagation constants β_{nm} and β'_{nm} of the TM and TE modes of the hollow waveguide, respectively).

3.4. The Transverse Fields at $\zeta = \zeta_1 + \zeta_2$

The expression $[1/(s^2+k^2h_{\zeta_1}^2)](sE_{r_0}^+ - j\omega\mu_0 H_{\theta_0}^+ h_{\zeta_1})$ in Equation (17a) for the first section of the flexible hollow waveguide with two bendings depends on the initial fields $E_{r_0}^+$ and $H_{\theta_0}^+$ (23a)–(23d). In the same principle we have the expression $[1/(s^2+k^2h_{\zeta_2}^2)](sE_r(\zeta=\zeta_1) - j\omega\mu_0 H_\theta(\zeta=\zeta_1)h_{\zeta_2})$ for the second section of the flexible hollow waveguide with two bendings, that depends on the output fields $E_r(\zeta=\zeta_1)$ and $H_\theta(\zeta=\zeta_1)$ (e.g., (24)) at $\zeta=\zeta_1$ of the first section. The inverse Laplace transform of this expression for the second section of the flexible hollow waveguide with two bendings is calculated by

$$\mathcal{L}^{-1}\left[\frac{1}{s^2+k^2h_{\zeta_2}^2}\left(sE_r(\zeta=\zeta_1)-j\omega\mu_0H_\theta(\zeta=\zeta_1)h_{\zeta_2}\right)\right]$$

$$= \mathcal{L}^{-1}\Bigg[\frac{s}{s^2+k^2h_{\zeta_2}^2}\Bigg(E_{r_0}^{+}e^{-jkh_{\zeta_1}\zeta_1} - \frac{j\omega\mu_0}{R_1}h_{\zeta_1}\cos^2\theta\sum_{m'}C_{S1}^{m'}(\zeta_1)J_1(\psi)$$
$$-\frac{j\omega\mu_0}{R_1}h_{\zeta_1}\sin\theta\cos\theta\sum_{m'}D_{S1}^{m'}(\zeta_1)J_1(\psi)+\frac{j\omega\mu_0}{r}h_{\zeta_1}^2\sin\theta\sum_{m'}C_{S1}^{m'}(\zeta_1)J_1(\psi)$$
$$-\frac{j\omega\mu_0}{r}h_{\zeta_1}^2\cos\theta\sum_{m'}D_{S1}^{m'}(\zeta_1)J_1(\psi)+\frac{1}{R_1}\sin\theta\cos\theta\sum_{m'}A_{S2}^{m'}(\zeta_1)J_1(\xi)$$
$$+\frac{1}{R_1}\sin^2\theta\sum_{m'}B_{S2}^{m'}(\zeta_1)J_1(\xi)+h_{\zeta_1}\cos\theta\sum_{m'}A_{S2}^{m'}(\zeta_1)\frac{dJ_1}{dr}(\xi)$$
$$+h_{\zeta 1}\sin\theta\sum_{m'}B_{S2}^{m'}(\zeta_1)\frac{dJ_1}{dr}(\xi)\Bigg)\Bigg] - \mathcal{L}^{-1}\Bigg[\frac{1}{s^2+k^2h_{\zeta_2}^2}(j\omega\mu_0h_{\zeta_2})$$
$$\Bigg(H_{\theta_0}^{+}e^{-jkh_{\zeta_1}\zeta_1} - \frac{j\omega\epsilon}{R_1}h_{\zeta_1}\sin\theta\cos\theta\sum_{m'}A_{S1}^{m'}(\zeta_1)J_1(\xi)$$
$$-\frac{j\omega\epsilon}{R_1}h_{\zeta_1}\sin^2\theta\sum_{m'}B_{S1}^{m'}(\zeta_1)J_1(\xi) - j\omega\epsilon h_{\zeta_1}^2\cos\theta\sum_{m'}A_{S1}^{m'}(\zeta_1)\frac{dJ_1}{dr}(\xi)$$
$$-j\omega\epsilon h_{\zeta_1}^2\sin\theta\sum_{m'}B_{S1}^{m'}(\zeta_1)\frac{dJ_1}{dr}(\xi)+\frac{1}{R_1}\cos^2\theta\sum_{m'}C_{S2}^{m'}(\zeta_1)J_1(\psi)$$
$$+\frac{1}{R_1}\sin\theta\cos\theta\sum_{m'}D_{S2}^{m'}(\zeta_1)J_1(\psi)-\frac{1}{r}h_{\zeta_1}\sin\theta\sum_{m'}C_{S2}^{m'}(\zeta_1)J_1(\psi)$$
$$+\frac{1}{r}h_{\zeta_1}\cos\theta\sum_{m'}D_{S2}^{m'}(\zeta_1)J_1(\psi)\Bigg)\Bigg]. \tag{28}$$

Note that

$$\mathcal{L}^{-1}\Bigg[\frac{s}{s^2+k^2h_{\zeta_2}^2}\Bigg(E_{r_0}^{+}e^{-jkh_{\zeta_1}\zeta_1}\Bigg)\Bigg]-\mathcal{L}^{-1}\Bigg[\frac{1}{s^2+k^2h_{\zeta_2}^2}(j\omega\mu_0h_{\zeta_2})\Bigg(H_{\theta_0}^{+}e^{-jkh_{\zeta_1}\zeta_1}\Bigg)\Bigg]$$
$$= \mathcal{L}^{-1}\Bigg[\frac{s}{s^2+k^2h_{\zeta_2}^2}\Bigg(\frac{2E_0}{n(r)+1}e^{-(r/w_o)^2}\sin\theta e^{-jkh_{\zeta_1}\zeta_1}\Bigg)\Bigg]$$
$$-\mathcal{L}^{-1}\Bigg[\frac{1}{s^2+k^2h_{\zeta_2}^2}(j\omega\mu_0h_{\zeta_1})\Bigg(\frac{2E_0}{n(r)+1}\frac{\eta}{\eta_0}e^{-(r/w_o)^2}\sin\theta e^{-jkh_{\zeta_1}\zeta_1}\Bigg)\Bigg]$$
$$= \cos(kh_{\zeta_2}\zeta_2)\Bigg(E_{r_0}^{+}e^{-jkh_{\zeta_1}}\Bigg) - \frac{\sin(kh_{\zeta_2}\zeta_2)}{kh_{\zeta_2}}\Bigg(jh_{\zeta_2}kE_{r_0}^{+}e^{-jkh_{\zeta_1}}\Bigg)$$
$$= E_{r_0}^{+}e^{-jk(r)(h_{\zeta_1}\zeta_1+h_{\zeta_2}\zeta_2)}, \tag{29}$$

where $E_r(\zeta = \zeta_1)$ and $H_\theta(\zeta = \zeta_1)$ are the output fields of the first section at $\zeta = \zeta_1$ and the beginning of the second section of the flexible hollow waveguide with two bendings (Fig. 1). Similarly, the other expressions for the second section of the flexible hollow waveguide with two bendings are given, by using the inverse Laplace transform.

The values of the input fields of the second section of the flexible hollow waveguide with two bendings are functions of the parameters of the first section (R_1, ζ_1, and h_{ζ_1}) and the second section (R_2, ζ_2, and h_{ζ_2}) as shown in Fig. 1. The expressions are functions of the parameters of the cross-section (r, θ) of the curved hollow waveguide, and the sum of the modes and the old coefficients of the first section of the curved waveguide with two bendings ($\sum_{m'} A_{S1}^{m'}(\zeta_1)J_1(\psi)J_1(\xi)\sin\theta\cos\theta$), where $\psi = [P'_{1m'}(r/a)]$, $\xi = [P_{1m'}(r/a)]$, $A_{S1}^{m'}(\zeta_1) = \mathcal{L}^{-1}[A_{1m'}(s)/(s^2 + k^2(r)h_{\zeta_1}^2)]$, $A_{S2}^{m'}(\zeta_1) = \mathcal{L}^{-1}[sA_{1m'}(s)/(s^2 + k^2(r)h_{\zeta_1}^2)]$, and $m' = 1, \ldots N$, where $3 \leq N \leq 50$.

The output transverse components of the fields are finally expressed in a form of *transfer matrix functions* as follows

$$
\begin{aligned}
&E_r(r,\theta,\zeta = \zeta_1 + \zeta_2) = E_{r_0}^{+} e^{-jk(r)(h_{\zeta_1}\zeta_1 + h_{\zeta_2}\zeta_2)} + \cos(kh_{\zeta_2}\zeta_2)\\
&\Bigg(-\frac{j\omega\mu_0}{R_1}h_{\zeta_1}\cos^2\theta\sum_{m'}C_{S1}^{m'}(\zeta_1)J_1(\psi) - \frac{j\omega\mu_0}{R_1}h_{\zeta_1}\sin\theta\cos\theta\sum_{m'}D_{S1}^{m'}(\zeta_1)J_1(\psi)\\
&+\frac{j\omega\mu_0}{r}h_{\zeta_1}^2\sin\theta\sum_{m'}C_{S1}^{m'}(\zeta_1)J_1(\psi) - \frac{j\omega\mu_0}{r}h_{\zeta_1}^2\cos\theta\sum_{m'}D_{S1}^{m'}(\zeta_1)J_1(\psi)\\
&+\frac{1}{R_1}\sin\theta\cos\theta\sum_{m'}A_{S2}^{m'}(\zeta_1)J_1(\xi) + \frac{1}{R_1}\sin^2\theta\sum_{m'}B_{S2}^{m'}(\zeta_1)J_1(\xi)\\
&+h_{\zeta 1}\cos\theta\sum_{m'}A_{S2}^{m'}\frac{dJ_1}{dr}(\xi) + h_{\zeta 1}\sin\theta\sum_{m'}B_{S2}^{m'}\frac{dJ_1}{dr}(\xi)\Bigg)\\
&-\frac{\sin(kh_{\zeta_2}\zeta_2)}{kh_{\zeta_2}}(j\omega\mu_0 h_{\zeta_2})\Bigg(-\frac{j\omega\epsilon}{R_1}h_{\zeta_1}\sin\theta\cos\theta\sum_{m'}A_{S1}^{m'}(\zeta_1)J_1(\xi)\\
&-\frac{j\omega\epsilon}{R_1}h_{\zeta_1}\sin^2\theta\sum_{m'}B_{S1}^{m'}(\zeta_1)J_1(\xi) - j\omega\epsilon h_{\zeta_1}^2\cos\theta\sum_{m'}A_{S1}^{m'}\frac{dJ_1}{dr}(\xi)\\
&-j\omega\epsilon h_{\zeta_1}^2\sin\theta\sum_{m'}B_{S1}^{m'}\frac{dJ_1}{dr}(\xi) + \frac{\cos^2\theta}{R_1}\sum_{m'}C_{S2}^{m'}(\zeta_1)J_1(\psi)
\end{aligned}
$$

$$+\frac{1}{R_1}\sin\theta\cos\theta\sum_{m'}D_{S2}^{m'}(\zeta_1)J_1(\psi)-\frac{1}{r}h_{\zeta_1}\sin\theta\sum_{m'}C_{S2}^{m'}(\zeta_1)J_1(\psi)$$

$$+\frac{1}{r}h_{\zeta_1}\cos\theta\sum_{m'}D_{S2}^{m'}(\zeta_1)J_1(\psi)\Bigg)-\frac{j\omega\mu_0}{R_2}h_{\zeta_2}\cos^2\theta\sum_{m'}C^{(2)}{}_{S1}^{m'}(\zeta_2)J_1(\psi)$$

$$-\frac{j\omega\mu_0}{R_2}h_{\zeta_2}\sin\theta\cos\theta\sum_{m'}D^{(2)}{}_{S1}^{m'}(\zeta_2)J_1(\psi)$$

$$+\frac{j\omega\mu_0}{r}h_{\zeta_2}^2\sin\theta\sum_{m'}C^{(2)}{}_{S1}^{m'}(\zeta_2)J_1(\psi)-\frac{j\omega\mu_0}{r}h_{\zeta_2}^2\cos\theta\sum_{m'}D^{(2)}{}_{S1}^{m'}(\zeta_2)J_1(\psi)$$

$$+\frac{1}{R_2}\sin\theta\cos\theta\sum_{m'}A^{(2)}{}_{S2}^{m'}(\zeta_2)J_1(\xi)+\frac{1}{R_2}\sin^2\theta\sum_{m'}B^{(2)}{}_{S2}^{m'}(\zeta_2)J_1(\xi)$$

$$+h_{\zeta_2}\cos\theta\sum_{m'}A^{(2)}{}_{S2}^{m'}(\zeta_2)\frac{dJ_1}{dr}(\xi)+h_{\zeta_2}\sin\theta\sum_{m'}B^{(2)}{}_{S2}^{m'}(\zeta_2)\frac{dJ_1}{dr}(\xi), \quad (30)$$

where $\psi=[P'_{1m'}(r/a)]$ and $\xi=[P_{1m'}(r/a)]$.

The new coefficients are given in the above equation, for instance

$$A^{(2)}{}_{S1}^{m'}(\zeta_2) = \mathcal{L}^{-1}\left[\frac{A^{(2)}{}_{1m'}(s)}{s^2+k^2(r)h_{\zeta_2}^2}\right], \quad (31a)$$

$$A^{(2)}{}_{S2}^{m'}(\zeta_2) = \mathcal{L}^{-1}\left[\frac{sA^{(2)}{}_{1m'}(s)}{s^2+k^2(r)h_{\zeta_2}^2}\right], \quad (31b)$$

where

$$m'=1,\dots N, \qquad 3\le N\le 50. \quad (31c)$$

Similarly, the other output transverse components of the fields are obtained, in a form of *transfer matrix functions* (e.g., Equation (30)). The above general solutions of the output transverse components of the fields (e.g., Equation (30)) at $\zeta=\zeta_1+\zeta_2$ are dependent on the initial fields at $\zeta=\zeta_1$ along the total length $\zeta=\zeta_1+\zeta_2$, where $\zeta_1=R_1\phi_1$ and $\zeta_2=R_2\phi_2$. Note that the main expression of the solution of the output transverse components of the fields (e.g., Equation (24)) is proportional to $E_{r_0}^{+}\exp[-jk(r)h_{\zeta_1}\zeta_1]$. In the same principle, the main expression for the second section of the flexible hollow waveguide with two bendings (e.g., Equation (30)) is proportional to $E_{r_0}^{+}\exp[-jk(r)(h_{\zeta_1}\zeta_1+h_{\zeta_2}\zeta_2)]$.

These above solutions (e.g., (30)) consist of the sum of the principle expression and other expressions. The principle expression is multiplication of the initial field at $\zeta=0^+$ (23a) with the exponent $[\exp[-jk(r)(h_{\zeta_1}\zeta_1+h_{\zeta_2}\zeta_2)]]$. All the above derivation is introduced in the case of the flexible hollow waveguide with two bendings in the same direction.

The inverse Laplace transform is performed in this study by a direct numerical integration in the Laplace transform domain by the residue method, as follows

$$f(\zeta)=\mathcal{L}^{-1}\left[\tilde{f}(s)\right]=\frac{1}{2\pi j}\int_{\sigma-j_\infty}^{\sigma+j_\infty}\tilde{f}(s)e^{s\zeta}ds=\sum_n \mathrm{Re}s\left[e^{s\zeta}\tilde{f}(s);S_n\right]. \quad (32)$$

By using the inverse Laplace transform (32) we can compute the output transverse components in the real plane and the output power density at each point at ζ. The integration path in the right side of the Laplace transform domain includes all the singularities according to Equation (32). All the points S_n are the poles of $\tilde{f}(s)$ and $\mathrm{Re}s[e^{s\zeta}\tilde{f}(s);S_n]$ represent the residue of the function in a specific pole. According to the residue method, two dominant poles for the toroidal waveguide are given by

$$s=\pm j\ k(r)h_\zeta=\pm j\ k(r)\left(1+\frac{r}{R}\sin\theta\right).$$

Finally, knowing all the transverse components, the ζ component of the average-power density Poynting vector is given by

$$S_{av}=\frac{1}{2}\mathrm{Re}\left\{E_rH_\theta{}^*-E_\theta H_r{}^*\right\}. \quad (33)$$

where the asterisk indicates the complex conjugate.

The total average-power transmitted along the guide in the ζ direction can now be obtained by the integral of Equation (33) over the waveguide cross section. Thus, the output power transmission is given by

$$T=\frac{1}{2}\int_0^{2\pi}\int_0^a \mathrm{Re}\left\{E_rH_\theta{}^*-E_\theta H_r{}^*\right\}rdrd\theta. \quad (34)$$

Lossy Medium Case

In a linear lossy medium, the solution is obtained by replacing the permittivity ϵ by $\epsilon_c=\epsilon-j(\sigma/\omega)$ in the preceding mathematical expressions, where ϵ_c is the complex dielectric constant and σ is the conductivity of the medium. The coefficients are obtained directly from the algebraic Equations (18a)–(18d) and are expressed as functions in the Laplace transform domain. To satisfy the metallic boundary conditions of a circular cross-section we find the new roots $P_{1m}^{(new)}$ and $P_{1m}^{'(new)}$ of the equations $J_1(z)=0$ and $dJ_1(z)/dz=0$, respectively, where z is complex. Thus, from the requirement that the coefficients vanish, the new roots $P_{1m}^{(new)}$ and $P_{1m}^{'(new)}$ are calculated by developing

into the Taylor series, in the first order at $1/\sigma$. The new roots in the case of a lossy medium are complex. The complex Bessel functions are computed by using NAG subroutine [22]. The explanation is given in detail in Ref. [14].

Several examples computed on a Unix system are presented in the next sections, in order to demonstrate the results of this proposed method for a toroidal waveguide and for small values of step angles. We suppose that the transmitted fields of the initial fields (TEM_{00} mode in excitation) are formulated by using the Fresnel coefficients (23a)–(23d).

4. NUMERICAL RESULTS

This section presents several examples that demonstrate features of the proposed mode model derived in the previous section. The cross-section (Fig. 6) of the curved waveguide is made of a tube of various types of material, a metallic layer, and a dielectric layer upon it. The next examples represent the case of the hollow waveguide with a metallic layer (Ag) coated by a thin dielectric layer (AgI). For silver having a conductivity of 6.14×10^7 $(\text{ohm} \cdot \text{m})^{-1}$ and the skin depth at 10.6 μm is 1.207×10^{-8} m.

Three test-cases are demonstrated for small values of the step's angle (δ_p). In these cases, $\delta_p \geq 2(a + \delta_m)/(2\pi R)$, according to the condition (2). Note that for small values of the step's angle, the helical waveguide becomes approximately a toroidal waveguide (see Fig. 2), where the radius of the curvature of the helix (ρ) can then be approximately by the radius of the cylinder (R).

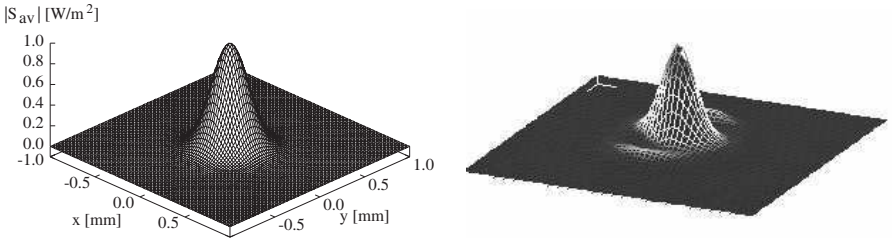

(a) (b)

Figure 8. The output power density ($a = 1\,\text{mm}$, $d_{(\text{AgI})} = 0.75\,\mu\text{m}$, $\lambda = 10.6\,\mu\text{m}$, $w_0 = 0.3\,\text{mm}$, $n_{(0)} = 1$, $n_{(\text{AgI})} = 2.2$, $n_{(\text{Ag})} = 13.5 - j75.3$, and the length of the straight waveguide is 1 m), for $R \to \infty$: (a) Theoretical result; (b) experimental result.

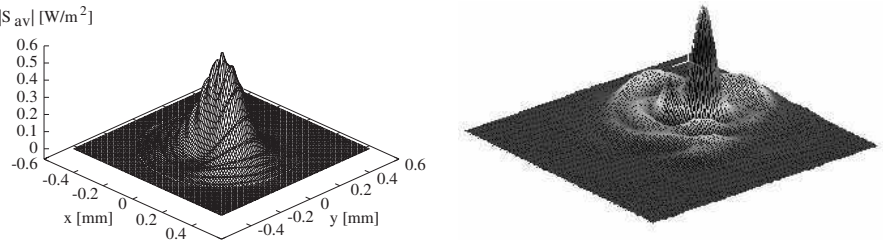

(a) (b)

Figure 9. Solution of the output power density ($a = 0.5\,\text{mm}$, $d_{(\text{AgI})} = 0.75\,\mu\text{m}$, $\lambda = 10.6\,\mu\text{m}$, $w_0 = 0.2\,\text{mm}$, $n_{(0)} = 1$, $n_{(\text{AgI})} = 2.2$, $n_{(\text{Ag})} = 13.5 - j75.3$, $R = 0.7\,\text{m}$, $\phi = \pi/2$, and $\zeta = 1\,\text{m}$): (a) Theoretical result; (b) experimental result.

The first test-case is demonstrated for the straight waveguide ($R \to \infty$). The results of the output transverse components of the fields and the output power density ($|S_{av}|$) (e.g., Fig. 8(a)) show the same behavior of the solutions as shown in the results of Ref. [14] for the TEM_{00} mode in excitation. The result of the output power density (Fig. 8(a)) is compared also to the result of published experimental data [23] (see also in Fig. 8(b)). This comparison shows good agreement (a Gaussian shape) as expected, except for the secondary small propagation mode. The experimental result (Fig. 8(b)) is influenced by the additional parameters (e.g., the roughness of the internal wall of the waveguide) which are not taken into account theoretically. In this example, the length of the straight waveguide is 1 m, the diameter (2a) of the waveguide is 2 mm, the thickness of the dielectric layer [$d_{(\text{AgI})}$] is 0.75 μm, and the minimum spot-size (w_0) is 0.3 mm. The refractive indices of the air, dielectric layer (AgI) and metallic layer (Ag) are $n_{(0)} = 1$, $n_{(\text{AgI})} = 2.2$, and $n_{(\text{Ag})} = 13.5 - j75.3$, respectively. The value of the refractive index of the material at a wavelength of $\lambda = 10.6\,\mu\text{m}$ is taken from the table compiled by Miyagi, et al. in Ref. [5].

The second test-case is demonstrated in Fig. 9(a) for the toroidal dielectric waveguide. Fig. 9(b) shows the experimental result that was received in the laboratory of Croitoru at Tel-Aviv University. This experimental result was obtained from the measurements of the transmitted CO_2 laser radiation ($\lambda = 10.6\,\mu\text{m}$) propagation through a hollow tube covered on the bore wall with silver and silver-iodide layers (Fig. 6), where the initial diameter (ID) is 1 mm (namely, small bore size).

The output modal profile is greatly affected by the bending, and the theoretical and experimental results (Figs. 9(a)–9(b)) show that in addition to the main propagation mode, several other secondary modes and asymmetric output shape appear. The amplitude of the output power density ($|S_{av}|$) is small as the bending radius (R) is small, and the shape is far from a Gaussian shape. This result agrees with the experimental results, but not for all propagation modes. The experimental result (Fig. 9(b)) is influenced by the bending and additional parameters (e.g., the roughness of the internal wall of the waveguide) which are not taken into account theoretically. In this

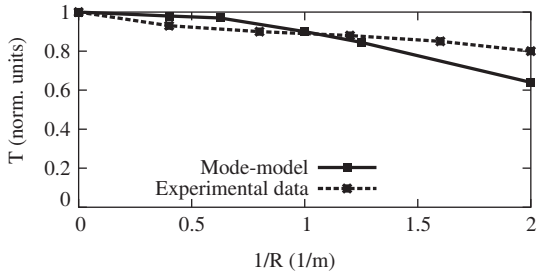

Figure 10. The theoretical mode-model's result and the experimental result [10] where the hollow metallic waveguide (Ag) is covered inside the walls with a AgI film. The output power transmission as a function of $1/R$ for $\delta_p = 0$, where $\zeta = 0.55\,\mathrm{m}$, where $a = 1.2\,\mathrm{mm}$, $d_{(\mathrm{AgI})} = 0.75\,\mu\mathrm{m}$, $w_0 = 0.1\,\mathrm{mm}$, $\lambda = 10.6\,\mu\mathrm{m}$, $n_{(0)} = 1$, $n_{(\mathrm{AgI})} = 2.2$, and $n_{(\mathrm{Ag})} = 10$.

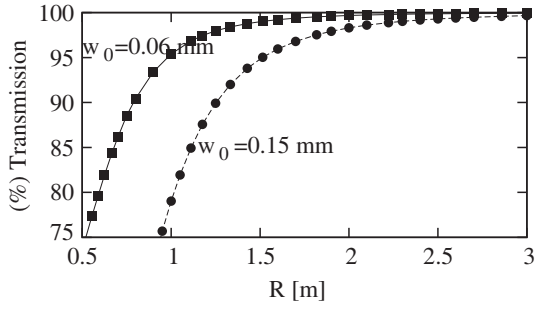

Figure 11. The output power transmission as a function of the radius of curvature for $\zeta_1 = 1\,\mathrm{m}$ in two cases of the spot size: (a) $w_0 = 0.06\,\mathrm{mm}$, (b) $w_0 = 0.15\,\mathrm{mm}$. The optimum result is obtained by the first solution of the first section of the flexible hollow waveguide.

example, $a = 0.5\,\text{mm}$, $R = 0.7\,\text{m}$, $\phi{=}\pi/2$, and $\zeta = 1\,\text{m}$. The thickness of the dielectric layer $[d_{(\text{AgI})}]$ is $0.75\,\mu\text{m}$ (Fig. 6), and the minimum spot size (w_0) is $0.2\,\text{mm}$. The values of the refractive indices of the air, dielectric layer (AgI) and metallic layer (Ag) are $n_{(0)} = 1$, $n_{(\text{AgI})} = 2.2$, and $n_{(\text{Ag})} = 13.5 - j75.3$, respectively. In both theoretical and experimental results (Figs. 9(a)–9(b)) the shapes of the output power density for the curved waveguide are not symmetric.

The third test-case is demonstrated in Fig. 10 for the toroidal dielectric waveguide. The theoretical mode-model's result and the experimental result [10] are demonstrated in normalized units where the length of the curved waveguide (ζ) is $0.55\,\text{m}$, the diameter $(2a)$ of the waveguide is $2.4\,\text{mm}$, and the minimum spot size (w_0) is $0.1\,\text{mm}$.

This comparison (Fig. 10) between the theoretical mode-model and the experimental data [10] indicates a good agreement. For all the examples, our theoretical mode-model takes into account only the dielectric losses and the bending losses, in conjunction with the problem of the propagation through a curved waveguide. The experimental result [10] takes into account additional parameters (e.g., the roughness of the internal wall of the waveguide) which are not taken into account theoretically. In spite of the differences, the comparison shows a good agreement. For small values of the bending $(1/R)$ in the case of small step's angle, the output power transmission is large and decreases with increasing the bending.

The next example represents the effect of the radius of the bending on the output power transmission for the first section of the toroidal waveguide. The output power transmission as a function of the radius of curvature is shown in Fig. 11 where the length of the first section of the flexible curved waveguide is $1\,\text{m}$, and where the values of the spot-size (w_0) are $0.06\,\text{mm}$ and $0.15\,\text{mm}$. The diameter $(2a)$ of the waveguide is $2\,\text{mm}$, and the value of the refractive index of the material at a wavelength of $\lambda = 10.6\,\mu\text{m}$. The output power transmission (T) is shown in Fig. 11 as an example for practical cases, where $75\% \leq T \leq 100\%$. The optimum result is obtain where the spot-size (w_0) is $0.06\,\text{mm}$.

Figures 12(a)–12(e) show the results of the output transverse components and the output power density of the field for $R_1 = 1\,\text{m}$ and for $R_2 = 0.9\,\text{m}$, where $a = 1\,\text{mm}$, $d_{(\text{AgI})} = 0.75\,\mu\text{m}$, $\lambda = 10.6\,\mu\text{m}$, $w_0 = 0.06\,\text{mm}$, $n_{(0)} = 1$, $n_{(\text{AgI})} = 2.2$, and $n_{(\text{Ag})} = 13.5 - j75.3$. By decreasing only the parameters of the radius of curvature to $R_1 = 0.7\,\text{m}$ and for $R_2 = 0.6\,\text{m}$, the results of the output transverse components and the output power density of the field are changed, as shown in Figs. 13(a)–13(e). The amplitude of the output power density in Fig. 13(e) is smaller than the amplitude of the output power density

in Fig. 12(e). The amplitude is small as the bending radius is small, and the shape is far from a Gaussian. The amplitude in Fig. 13(e) is smaller as regart to the case of straight waveguide, but the amplitude in Fig. 12(e) is closer to the result in the case of the straight waveguide. The output results are greatly affected by the bending, and by the spot size (w_0). This mode model will be a useful tool in order to determine the optimal conditions for practical applications (output fields, output power density and output power transmission as function of the bending).

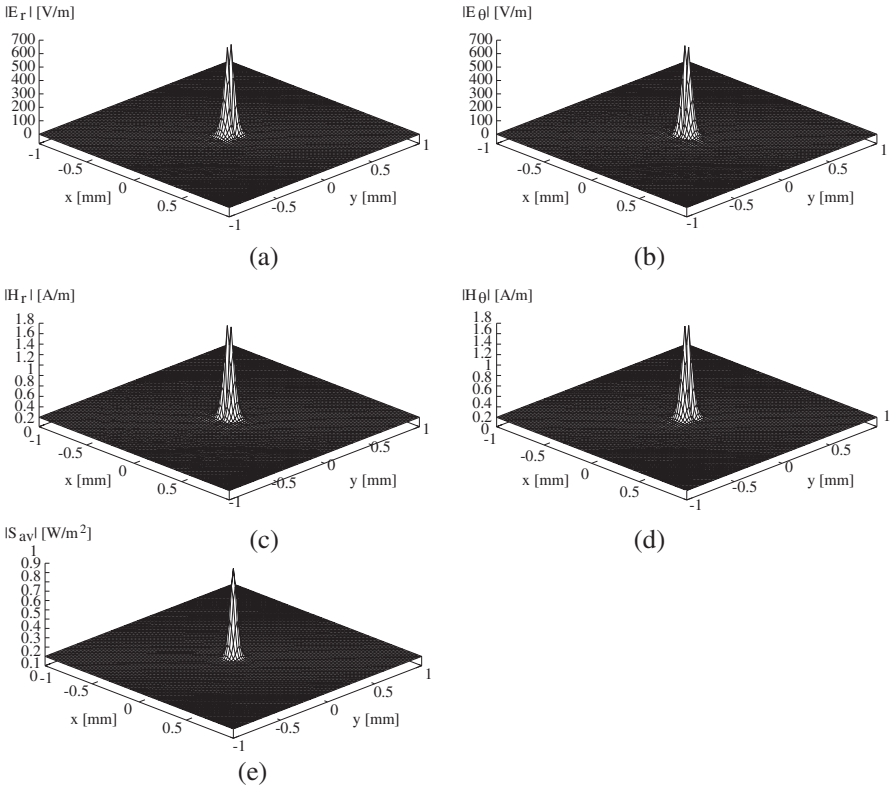

Figure 12. (a)–(d) The solution of the output transverse components, and (e) the output power density, in the case of the flexible toroidal waveguide with the two bendings, where $R_1 = 1\,\mathrm{m}$ and $R_2 = 0.9\,\mathrm{m}$, $a = 1\,\mathrm{mm}$, $d_{(\mathrm{AgI})} = 0.75\,\mu\mathrm{m}$, $\lambda = 10.6\,\mu\mathrm{m}$, $w_0 = 0.06\,\mathrm{mm}$, $n_{(0)} = 1$, $n_{(\mathrm{AgI})} = 2.2$, and $n_{(\mathrm{Ag})} = 13.5 - j75.3$.

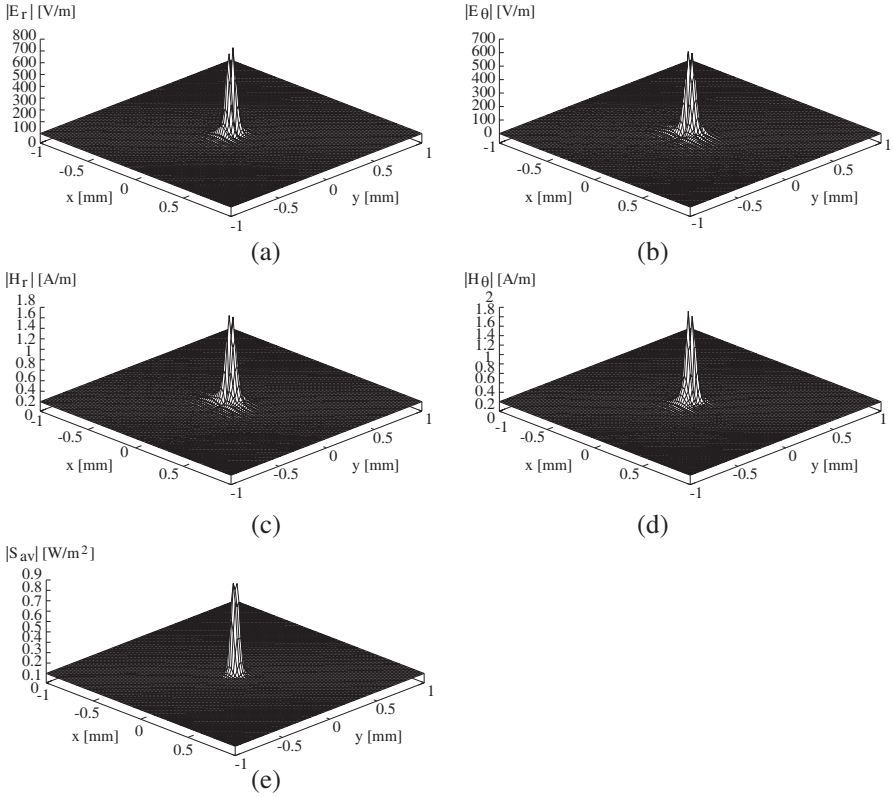

Figure 13. (a)–(d) The solution of the output transverse components, and (e) the output power density, in the case of the flexible toroidal waveguide with the two bendings, where $R_1 = 0.7\,\mathrm{m}$ and $R_2 = 0.6\,\mathrm{m}$, $a = 1\,\mathrm{mm}$, $d_{(\mathrm{AgI})} = 0.75\,\mu\mathrm{m}$, $\lambda = 10.6\,\mu\mathrm{m}$, $w_0 = 0.06\,\mathrm{mm}$, $n_{(0)} = 1$, $n_{(\mathrm{AgI})} = 2.2$, and $n_{(\mathrm{Ag})} = 13.5 - j75.3$.

5. CONCLUSION

The main objective was to generalize the method [14] to provide a numerical tool for the calculation of the output transverse fields and power density in the case of the flexible hollow waveguide that consists of two bendings in the same direction, as shown in Fig. 1. The main steps of the method for the two bendings are given in the derivation, in detail, for small values of step angles. Note that for small values of the step's angle, the helical waveguide becomes approximately a toroidal waveguide (see Fig. 2), where the radius of the curvature of the helix (ρ) can then be approximately by the radius of the cylinder (R).

Three test-cases were demonstrated for small values of the step's angle. The first test-case was demonstrated for the straight waveguide ($R \rightarrow \infty$). The results of the output transverse components of the fields and the output power density ($|S_{av}|$) (e.g., Fig. 8(a)) show the same behavior of the solutions as shown in the results of Ref. [14] for the TEM_{00} mode in excitation. The result of the output power density (Fig. 8(a)) was compared also to the result of published experimental data [23] (see also in Fig. 8(b)). This comparison shows good agreement (a Gaussian shape) as expected, except for the secondary small propagation mode. The experimental result (Fig. 8(b)) is influenced by the additional parameters (e.g., the roughness of the internal wall of the waveguide) which are not taken into account theoretically.

The second test-case was demonstrated in Fig. 9(a) for the toroidal dielectric waveguide, and Fig. 9(b) shows the experimental result. The output modal profile is greatly affected by the bending, and the theoretical and experimental results (Figs. 9(a)–9(b)) show that in addition to the main propagation mode, several other secondary modes and asymmetric output shape appear. The amplitude of the output power density ($|S_{av}|$) is small as the bending radius (R) is small, and the shape is far from a Gaussian shape. This result agrees with the experimental results, but not for all propagation modes. The experimental result (Fig. 9(b)) is influenced by the bending and additional parameters (e.g., the roughness of the internal wall of the waveguide) which are not taken into account theoretically. In both theoretical and experimental results (Figs. 9(a)–9(b)) the shapes of the output power density for the curved waveguide are not symmetric.

The third test-case was demonstrated in Fig. 10 for the toroidal dielectric waveguide. This comparison (Fig. 10) between the theoretical mode-model and the experimental data [10] indicates a good agreement. For all the examples, our theoretical mode-model takes into account only the dielectric losses and the bending losses, in conjunction with the problem of the propagation through a curved waveguide. The experimental result [10] takes into account additional parameters (e.g., the roughness of the internal wall of the waveguide) which are not taken into account theoretically. In spite of the differences, the comparison shows a good agreement. For small values of the bending ($1/R$) in the case of small step's angle, the output power transmission is large and decreases with increasing the bending.

The output power transmission as a function of the radius of curvature is shown in Fig. 11 where the length of the first section of the flexible curved waveguide is 1 m, and where the values of the spot-size (w_0) are 0.06 mm and 0.15 mm. The optimum result is obtain

where the spot-size (w_0) is 0.06 mm. Figs. 12(a)–12(e) show the results of the output transverse components and the output power density of the field where $R_1 = 1\,\mathrm{m}$ and for $R_2 = 0.9\,\mathrm{m}$, where $a = 1\,\mathrm{mm}$, $d_{(\mathrm{AgI})} = 0.75\,\mu\mathrm{m}$, $\lambda = 10.6\,\mu\mathrm{m}$, $w_0 = 0.06\,\mathrm{mm}$, $n_{(0)} = 1$, $n_{(\mathrm{AgI})} = 2.2$, and $n_{(\mathrm{Ag})} = 13.5 - j75.3$. By decreasing only the parameters of the radius of curvature to $R_1 = 0.7\,\mathrm{m}$ and for $R_2 = 0.6\,\mathrm{m}$, the results of the output transverse components and the output power density of the field are changed, as shown in Figs. 13(a)–13(e).

The amplitude of the output power density in Fig. 13(e) is smaller as regart to the amplitude of the output power density in Fig. 12(e). The amplitude is small as the bending radius is small, and the shape is far from a Gaussian. The amplitude in Fig. 13(e) is smaller than that in the case of straight waveguide, but the amplitude in Fig. 12(e) is closer to the result in the case of the straight waveguide. The output results are greatly affected by the bending, and by the spot size (w_0). This mode model will be a useful tool in order to determine the optimal conditions for practical applications (output fields, output power density and output power transmission as function of the bending), in all the cases of the hollow toroidal waveguides, e.g., in medical and industrial regimes.

APPENDIX A.

By using the Serret-Frenet relations for a spatial curve, we can find the curvature (κ) and the torsion (τ) for each spatial curve that is characterized by $\theta = \text{const}$ and $r = \text{const}$ for each pair (r, θ) in the range. This is achieved by using the helical transformation introduced in Equations (3a)–(3c).

The location vector for the helical transformation of the coordinates (1) is given by

$$\begin{aligned}\mathbf{r} \;=\; & \Big((R + r\sin\theta)\cos(\phi_c) + r\sin(\delta_p)\cos\theta\sin(\phi_c)\Big)\hat{i} \\ & + \Big((R + r\sin\theta)\sin(\phi_c) - r\sin(\delta_p)\cos\theta\cos(\phi_c)\Big)\hat{j} \\ & + \Big(r\cos\theta\cos(\delta_p) + R\phi_c\tan(\delta_p)\Big)\hat{k}, \qquad \text{(A1)}\end{aligned}$$

where $\phi_c = (\zeta/R)\cos(\delta_p)$, R is the radius of the cylinder, and (r, θ) are the parameters of the cross-section.

The tangent vector is given by $\mathbf{T} = (d\mathbf{r}/d\zeta) = (d\mathbf{r}/d\phi_c)/(d\zeta/d\phi_c)$,

The normal vector is given by $\mathbf{N} = (1/\kappa)(d\mathbf{T}/d\zeta)$, and the binormal vector is given by $\mathbf{B} = \mathbf{T} \times \mathbf{N}$.

The rate of the change of the tangent vector related to the parameter ζ measures the curvature, and is given by $d\mathbf{T}/d\zeta = (d\mathbf{T}/d\phi_c)/(d\zeta/d\phi_c)$.

The curvature of the helix is constant for constant values of the radius of the cylinder (R), the step's angle (δ_p) and the parameters (r, θ) of the cross-section. The curvature is given by the first Serret-Frenet equation of a curve $r(\zeta)$ in the space according to $d\mathbf{T}/d\zeta = \kappa\mathbf{N}$. Thus, the curvature is

$$\kappa = \left|\frac{d\mathbf{T}}{d\zeta}\right| = \frac{1 + C_t}{R(1 + \tan^2(\delta_p) + C_t)}, \qquad (A2)$$

where

$$C_t = \frac{r^2}{R^2}\sin^2\theta + 2\frac{r}{R}\sin\theta + \frac{r^2}{R^2}\sin^2(\delta_p)\cos^2\theta,$$

and the radius of curvature is given by $\rho = 1/\ \kappa$.

The rate of the change of the binormal vector related to the parameter ζ measures the torsion, and is given by $d\mathbf{B}/d\zeta = (d\mathbf{B}/d\phi_c)/(d\zeta/d\phi_c)$.

The torsion of the helix is constant for constant values of the radius of the cylinder (R), the step's angle (δ_p) and the parameters (r, θ) of the cross-section. The torsion is given by the second Serret-Frenet equation of a curve $r(\zeta)$ in the space according to $d\mathbf{B}/d\zeta = -\tau\mathbf{N}$. Thus, the torsion is

$$\tau = \left|\frac{d\mathbf{B}}{d\zeta}\right| = \frac{\tan\delta_p}{R(1 + \tan^2(\delta_p) + C_t)}, \qquad (A3)$$

where C_t is given above, and the radius of torsion is given by $\sigma = 1/\tau$.

APPENDIX B.

The elements of the matrices ($G_{00}^{(1)mm'}$, etc.) are given by:

$$G_{00}^{(1)mm'} = \int_0^a J_1\left(P_{1m'}\frac{r}{a}\right) J_1\left(P_{1m}\frac{r}{a}\right) r dr \delta_{1n},$$

$$G_{01}^{(1)mm'} = \int_0^a g(r) J_1\left(P_{1m'}\frac{r}{a}\right) J_1\left(P_{1m}\frac{r}{a}\right) r dr \delta_{1n},$$

$$G_{02}^{(1)mm'} = \int_0^a J_1\left(P_{1m'}\frac{r}{a}\right) J_1\left(P_{1m}\frac{r}{a}\right) r^3 dr \delta_{1n},$$

$$G_{03}^{(1)mm'} = \int_0^a g(r) J_1\left(P_{1m'}\frac{r}{a}\right) J_1\left(P_{1m}\frac{r}{a}\right) r^3 dr\delta_{1n},$$

$$G_{04}^{(1)mm'} = \int_0^a g^2(r) J_1\left(P_{1m'}\frac{r}{a}\right) J_1\left(P_{1m}\frac{r}{a}\right) r^3 dr\delta_{1n},$$

$$G_{05}^{(1)mm'} = \int_0^a k^2 g(r) J_1\left(P_{1m'}\frac{r}{a}\right) J_1\left(P_{1m}\frac{r}{a}\right) r dr\delta_{1n},$$

$$G_{08}^{(1)mm'} = \int_0^a g_r\left(\frac{P_{1m'}}{a}\right) {J_1}'\left(P_{1m'}\frac{r}{a}\right) J_1\left(P_{1m}\frac{r}{a}\right) r dr,$$

$$G_{09}^{(1)mm'} = \int_0^a g_r J_1\left(P_{1m'}\frac{r}{a}\right) J_1\left(P_{1m}\frac{r}{a}\right) r^2 dr\delta_{1n},$$

$$G_{10}^{(1)mm'} = \int_0^a {J_1}'\left(\frac{P_{1m'}r}{a}\right) J_1\left(P_{1m}\frac{r}{a}\right) r^2 dr\delta_{1n},$$

$$G_{11}^{(1)mm'} = \int_0^a g_r {J_1}'\left(\frac{P_{1m'}r}{a}\right) J_1\left(P_{1m}\frac{r}{a}\right) r^3 dr\delta_{1n},$$

$$G_{13}^{(1)mm'} = \int_0^a g_r {J_1}'\left(\frac{p'_{1m'}r}{a}\right) J_1\left(P_{1m}\frac{r}{a}\right) dr\delta_{1n},$$

$$G_{14}^{(1)mm'} = \int_0^a g_r J_1\left(\frac{p'_{1m'}r}{a}\right) J_1\left(P_{1m}\frac{r}{a}\right) r^2 dr\delta_{1n},$$

$$G_{15}^{(1)mm'} = \int_0^a J_1\left(P'_{1m'}\frac{r}{a}\right) J_1\left(P_{1m}\frac{r}{a}\right) r dr\delta_{1n},$$

$$G_{16}^{(1)mm'} = \int_0^a {J_1}'\left(\frac{P'_{1m'}r}{a}\right) J_1\left(P_{1m}\frac{r}{a}\right) r^2 dr\delta_{1n},$$

Similarly, the remaining elements are obtained. The coefficients are obtained directly from the algebraic system of Equations (18a)–(18d) and are expressed as functions in s-plane. Similarly, the other coefficients are obtained.

REFERENCES

1. Harrington, J. A. and Y. Matsuura, "Review of hollow waveguide technology," *Biomedical Optoelectronic Instrumentation*,

A. Katzir, J. A. Harrington, and D. M. Harris (eds.), *SPIE*, Vol. 2396, 4–14, 1995.

2. Harrington, J. A., "A review of IR transmitting, hollow waveguides," *Fiber and Integrated Optics*, Vol. 19, 211–228, 2000.
3. Marcatili, E. A. J. and R. A. Schmeltzer, "Hollow metallic and dielectric waveguides for long distance optical transmission and lasers," *Bell Syst. Tech. J.*, Vol. 43, 1783–1809, 1964.
4. Marhic, M. E., "Mode-coupling analysis of bending losses in IR metallic waveguides," *Appl. Opt.*, Vol. 20, 3436–3441, 1981.
5. Miyagi, M., K. Harada, and S. Kawakami, "Wave propagation and attenuation in the general class of circular hollow waveguides with uniform curvature," *IEEE Trans. Microwave Theory Tech.*, Vol. 32, 513–521, 1984.
6. Croitoru, N., E. Goldenberg, D. Mendlovic, S. Ruschin, and N. Shamir, "Infrared chalcogenide tube waveguides," *SPIE*, Vol. 618, 140–145, 1986.
7. Melloni, A., F. Carniel, R. Costa, and M. Martinelli, "Determination of bend mode characteristics in dielectric waveguides," *J. Lightwave Technol.*, Vol. 19, 571–577, 2001.
8. Bienstman, P., M. Roelens, M. Vanwolleghem, and R. Baets, "Calculation of bending losses in dielectric waveguides using eigenmode expansion and perfectly matched layers," *IEEE Photon. Technol. Lett.*, Vol. 14, 164–166, 2002.
9. Mendlovic, D., E. Goldenberg, S. Ruschin, J. Dror, and N. Croitoru, "Ray model for transmission of metallic-dielectric hollow bent cylindrical waveguides," *Appl. Opt.*, Vol. 28, 708–712, 1989.
10. Morhaim, O., D. Mendlovic, I. Gannot, J. Dror, and N. Croitoru, "Ray model for transmission of infrared radiation through multibent cylindrical waveguides," *Opt. Eng.*, Vol. 30, 1886–1891, 1991.
11. Kark, K. W., "Perturbation analysis of electromagnetic eigenmodes in toroidal waveguides," *IEEE Trans. Microwave Theory Tech.*, Vol. 39, 631–637, 1991.
12. Lewin, L., D. C. Chang, and E. F. Kuester, *Electromagnetic Waves and Curved Structures*, Ch. 6, 58–68, Peter Peregrinus Ltd., London, 1977.
13. Menachem, Z., "Wave propagation in a curved waveguide with arbitrary dielectric transverse profiles," *Progress In Electromagnetics Research*, PIER 42, 173–192, 2003.
14. Menachem, Z., N. Croitoru, and J. Aboudi, "Improved mode

model for infrared wave propagation in a toroidal dielectric waveguide and applications," *Opt. Eng.*, Vol. 41, 2169–2180, 2002.

15. Menachem, Z. and M. Mond, "Infrared wave propagation in a helical waveguide with inhomogeneous cross section and applications," *Progress In Electromagnetics Research*, PIER 61, 159–192, 2006.
16. Menachem, Z. and M. Haridim, "Propagation in a helical waveguide with inhomogeneous dielectric profiles in rectangular cross section," *Progress In Electromagnetics Research B*, Vol. 16, 155–188, 2009.
17. Collin, R. E., *Foundation for Microwave Engineering*, McGraw-Hill, New York, 1996.
18. Yariv, A., *Optical Electronics*, 3rd edition, Holt-Saunders Int. Editions, 1985.
19. Baden Fuller, A. J., *Microwaves*, Ch. 5, 118–120, A. Wheaton and Co. Ltd, Pergamon Press, Oxford, 1969.
20. Olver, F. W. J., *Royal Society Mathematical Tables, Zeros and Associated Values*, 2–30, University Press Cambridge, 1960.
21. Jahnke, E. and F. Emde, *Tables of Functions with Formulae and Curves*, Ch. 8, 166, Dover publications, New York, 1945.
22. The Numerical Algorithms Group (NAG) Ltd., Wilkinson House, Oxford, UK.
23. Croitoru, N., A. Inberg, M. Oksman, and M. Ben-David, "Hollow silica, metal and plastic waveguides for hard tissue medical applications," *SPIE*, Vol. 2977, 30–35, 1997.